## I JONIKA

### Įvadas

**1. SUPERJONINIŲ KRISTALŲ STRUKTŪROS**

1.1.Retoji jonų sanglauda Ag+ superjonikų kristalinėse struktūrose

1.2.Kristalinės $V_O^{\cdot\cdot}$, Na+, H+ superjonikų struktūros

1.3.Netvarkios Li+ superjonikų struktūros

**2. JONINIS SUPERJONIKŲ LAIDUMAS IR** POLIARIZACINIAI REIŠKINIAI

2.1. Taškiniai Frenkelio ir Šotkio defektai superjonikuose.

2.2. Stabilizuojančiųjų Y2O3 priemaišų įtaka elektrinėms ZrO2 keramikų savybėms

**3. SUPERJONINIŲ JUNGINIŲ ELEKTRINIŲ SAVYBIŲ TYRIMO METODAI**

3.1.Joninio laidumo sando ir dielektrinės skvarbos tyrimo metodai elektriniuose žemojo ir aukštojo dažnių laukuos

3.2. Superjonikų elektrinių savybių tyrimo metodai mikrobangiuose elektriniuose laukuose

**4. DINAMINĖS SUPERJONIKŲ SAVYBĖS**

4.1.Dielektrinės skvarbos ir elektrinio joninių ir superjoninių kristalų laidumo prieklausų nuo elektrinio lauko dažnio aprašas

4.2.Relaksacinė superjonikų joninio laidumo dispersija

4.3.Relaksacinė ir rezonansinė $\sigma$ ir $\varepsilon$ dispersijos Li+ superjonikuose

**5. SUPERJONINIŲ JUNGINIŲ TAIKYMAS**

Superjoniniai akumuliatoriai

.Kuro gardelės

Deguonies siurbliai

Deguonies dujų jutikliai

Anglies monoksido dujų jutikliai

Anglies dioksido dujų jutikliai

Jonistoriai

**Literatūra**


1. Tetsuichi Kudo and Kazuo Fueki "*Solid StateiIonics*", Kadansha, 1990.
2. M.B. Salamon "*Physics of Superionic Conductors*", Springer-Verlag Berlin Heidelberg, New York, 1979.
3. V. Grivickas, A,F.Orliukas, A. Žindulis, S. Tamulevičius, Medžiagų mokslas, Progretus, Vilnius, 2008.
4. A.F. Orliukas, "*Superjoniniai laidininkai*", Vilnius, VUL, 2004.
5. V.V.Kharton, „Solid State Electrochemistry I", Fundamentals, Materials and their Applications, Wiley-Vch Verlag GmbH&Co. KGaA,2009.
6. John O'M. Bockris, Amulys K. N. Reddy, Maria Gambos- Aldeco, *Modern Electrochemistry* (*Fundamentals of electrodics)*, (Kluwer academic publishers, New York, Boston, Doldrecht, London, Moscow, 2002).
7. Anthony R. West „ Solid State Chemistry and its Applications", John Wiley & Sons Ltd., Reprinted 1990.
8. A.K. Jonscher „Dielectric relaxation in solids", Chelsea Dielectrcs Press, London, 1996.
9. F. A. Karamov, „Superionic Conductors, Cambidge International Science Publishing,2008.
10. J.Kawamura, S. Yoshikado, T. sakuma, Y. Michihiro, M. Aniya, Y. Ito, „Superionic Conductor Physics",World Scientific, 2007.



**Paruošė prof. A.F.Orliukas**

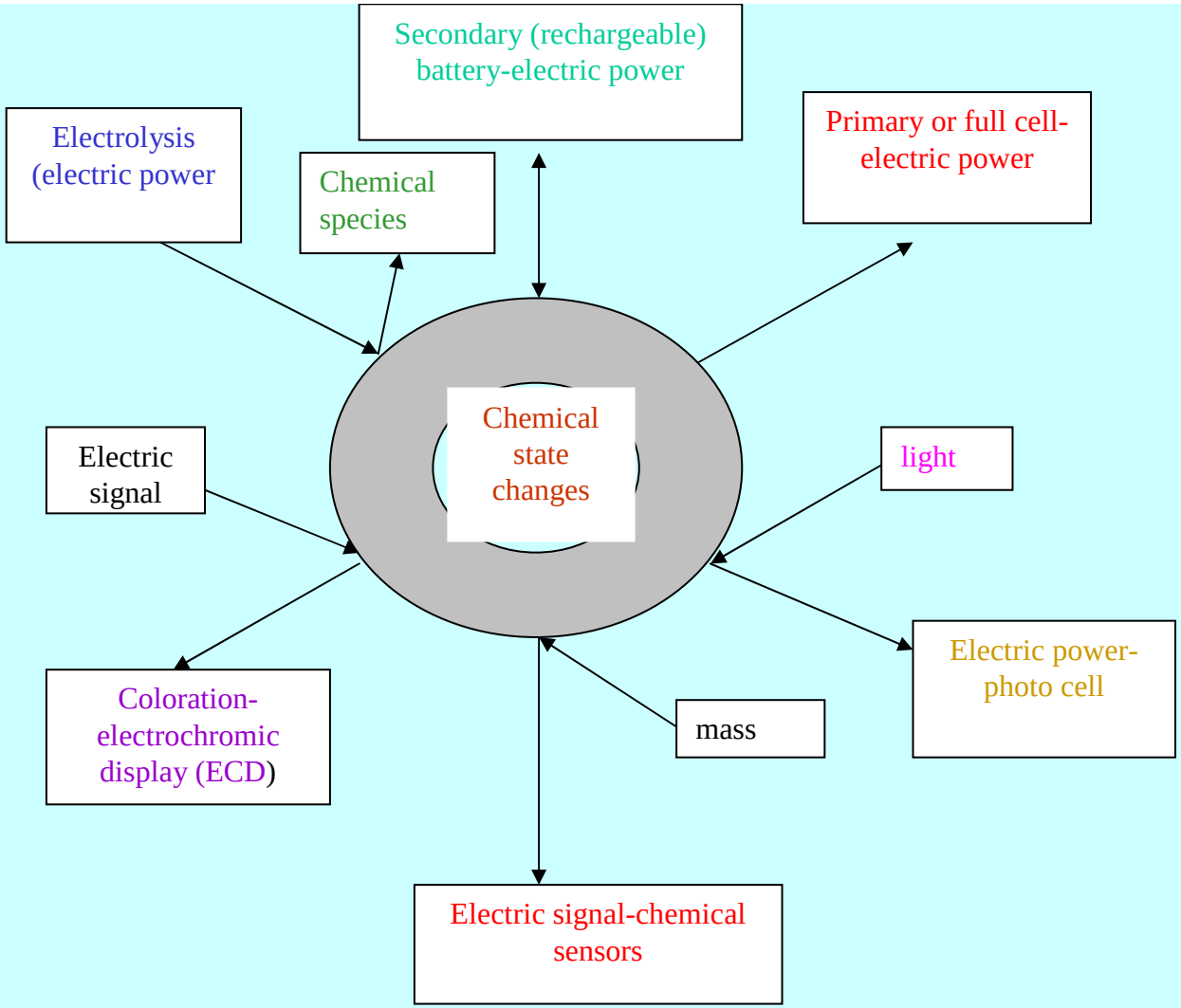


**Electrochemical devices**
**agree T. Kudo, K. Fueki, SSI, 1990**

| | |
|---|---|
| **1833** | **Faraday's Law** |
| **1897** | **$ZrO_2$ glower (Nernst)** |
| **1920** | **High ionic conduction in α-AgI** |
| **1933** | **Diffusion theory of lattice defects** |
| **1934** | **Ion transport mechanism for α-AgI** |
| **1943** | **Ionic conduction theory for $ZrO_2$** |
| **1962** | **High temperature fuel cell using $ZrO_2$** |
| **1967** | **β-alumina, Rb $Ag_4I_5$** |
| **1969** | **Electro-chromism in $WO_3$** |
| **1970** | **Electric double-layer capacitors (ionistor)** |
| **1970** | **Electrochemical memory devices** |
| **1972** | **Solid state Li battery, memoriode** |
| **1976** | **NASICON**<br>**secondary battery using $TiS_2$**<br>**intercalation** |
| **1979** | **High $Cu^+$ conductor**<br>**Organic polymer solid-electrolyte** |
| **1981** | **Plastic battery** |
| **1983** | **Commercial ECD** |
| **Future prospects of SSI**<br>**Neuron fiber** | |
| **Bio-computer system** | |

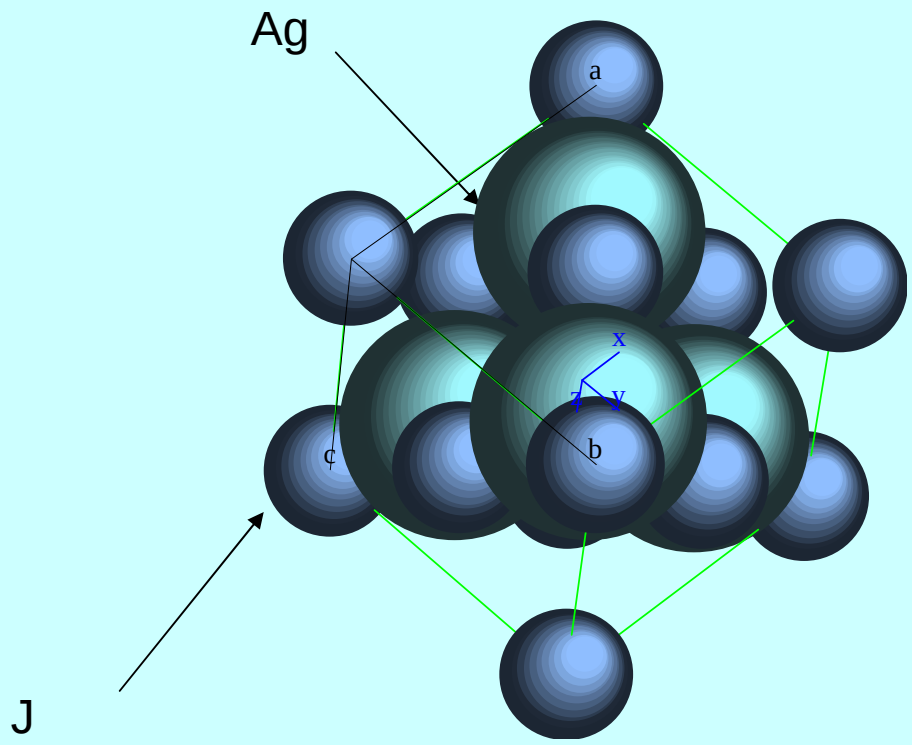


α–AgJ structure

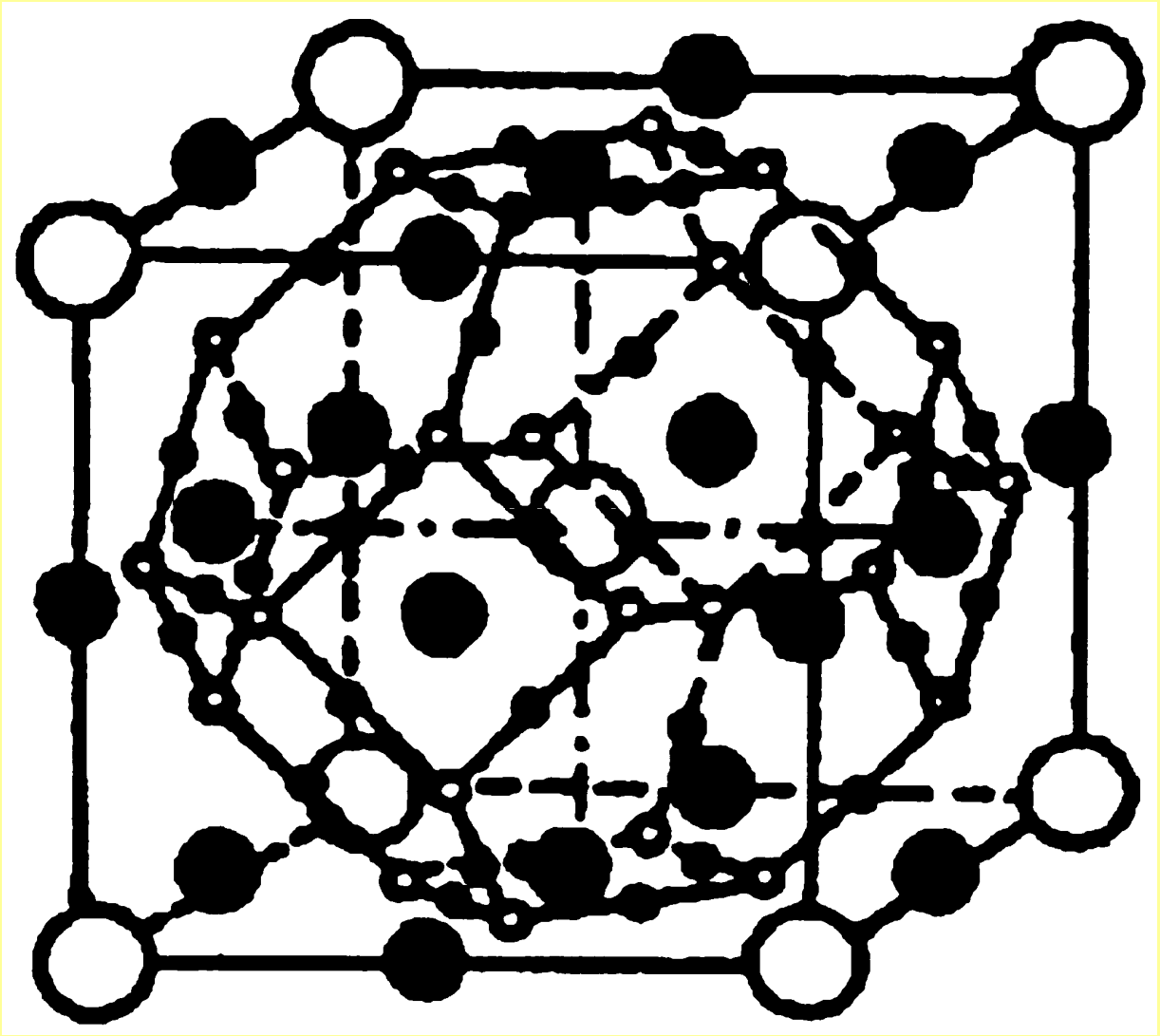

J d h b

α–AgJ lattice

In the lattice of $\alpha$-AgI are d-12, b-6 and h-24 energy positions for diffusion of 2 Ag ions.

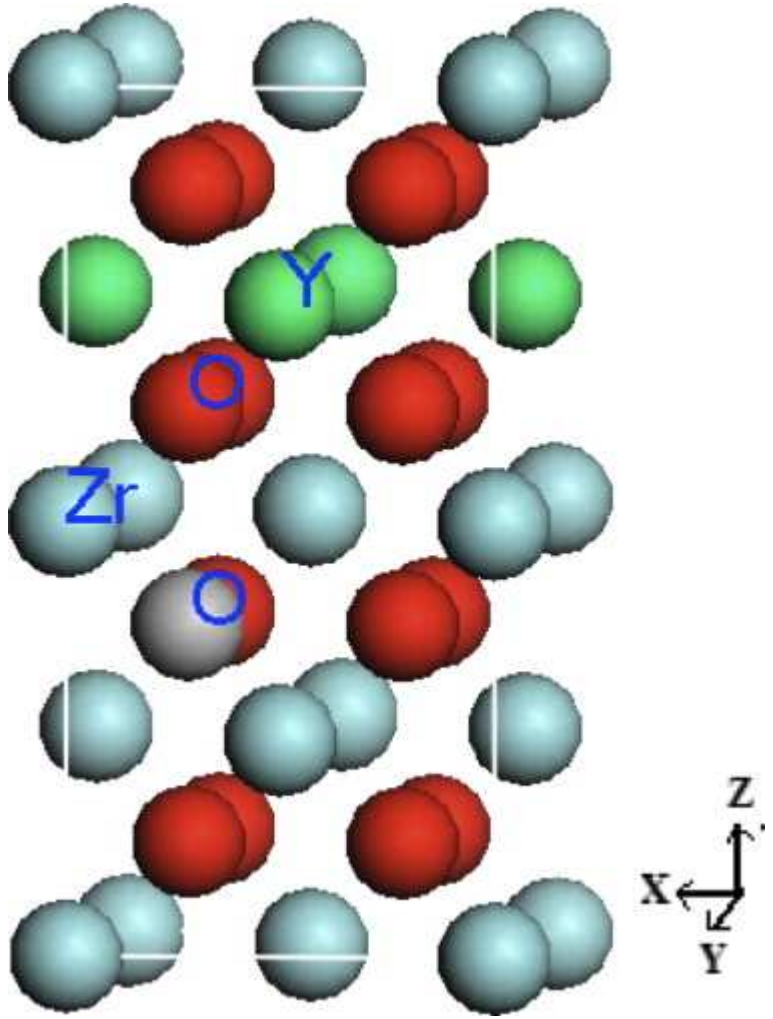


YSZ

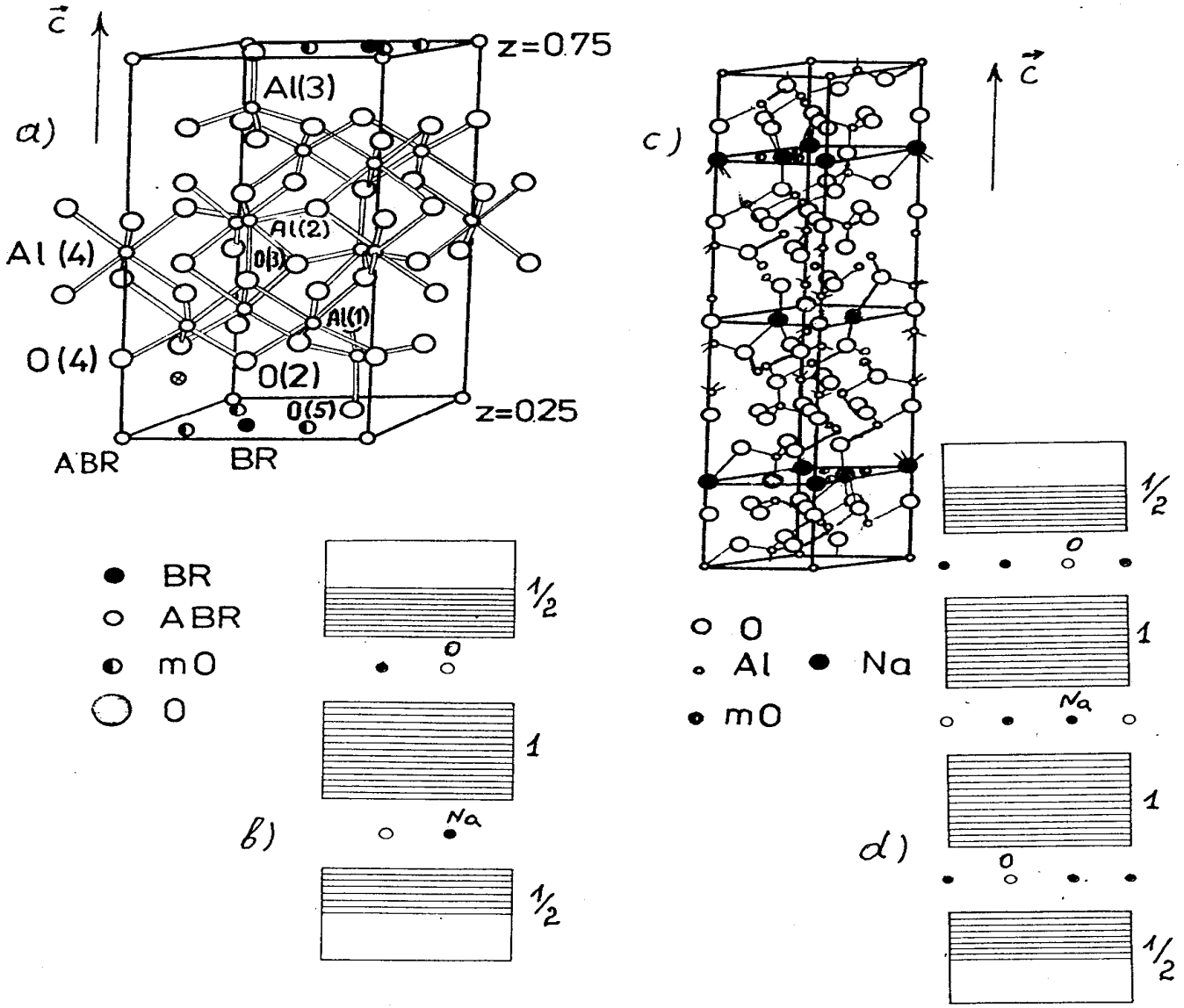
a)
c
z=0.75
Al(3)
Al(2)
Al (4)
O(3)
Al(1)
O(4)
O(2)
O(5)
z=0.25
ABR
BR
BR
ABR
mO
O
b)
1/2
O
1
Na
1/2
c)
c
O
Al
Na
mO
1/2
O
1
Na
d)
1
O
1/2

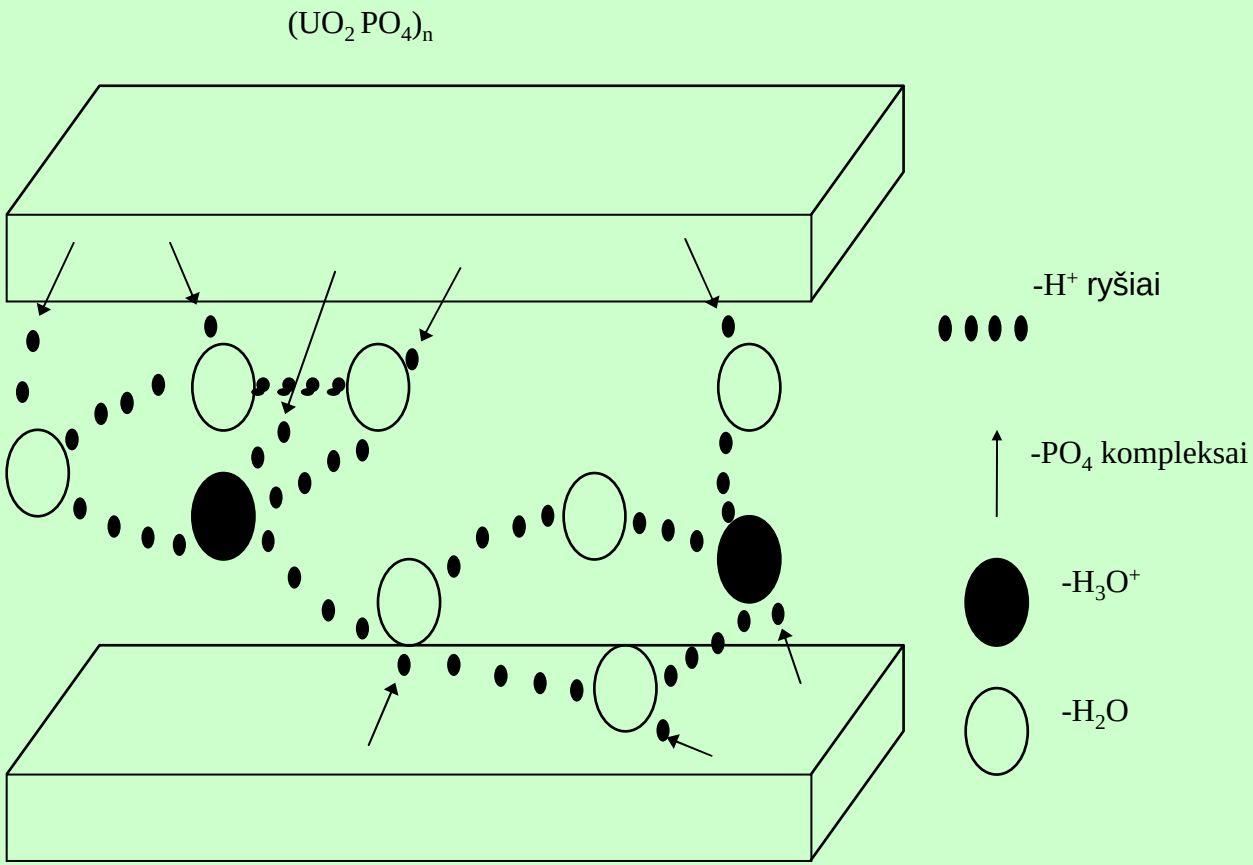


HUP structure

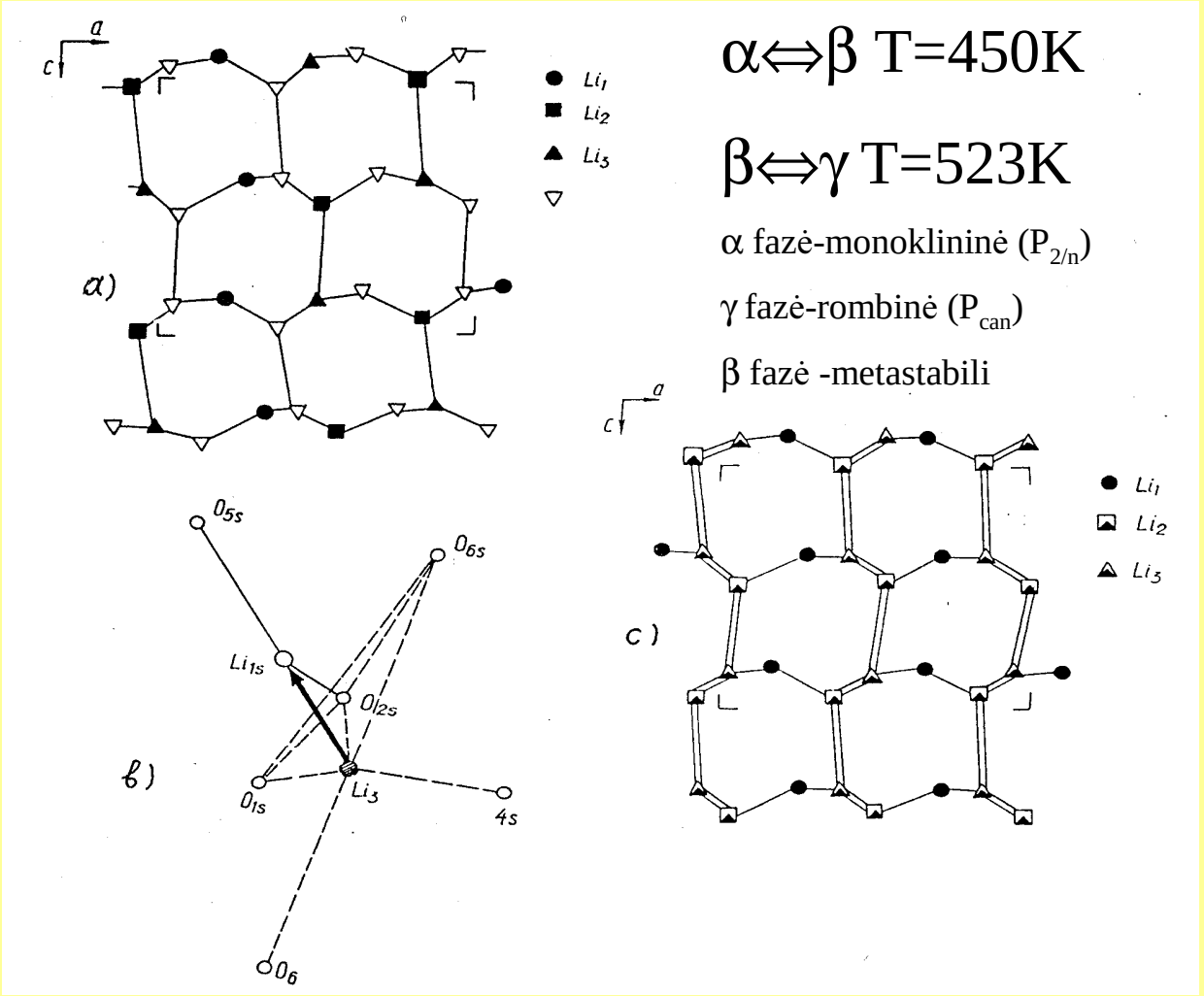


$\alpha \Leftrightarrow \beta$ T=450K

$\beta \Leftrightarrow \gamma$ T=523K

$\alpha$ fazė-monoklininė ($P_{2/n}$)

$\gamma$ fazė-rombinė ($P_{can}$)

$\beta$ fazė -metastabili

a) $\alpha$-$Li_3Fe_2(PO_4)_3$ $Li^+$ ion map on the (010) plane, b) oxygen window in $\beta$ phase on the (001) plane, c) $\gamma$ - $Li_3Fe_2(PO_4)_3$ $Li^+$ ion map on the (010) plane

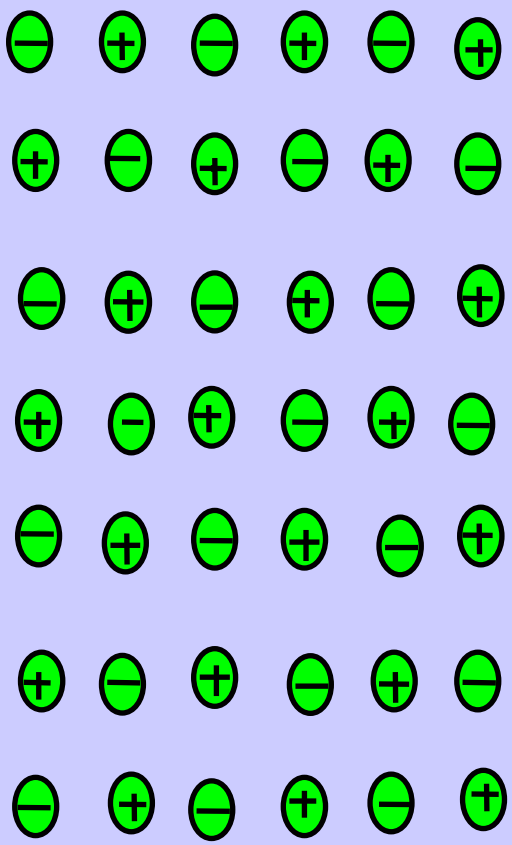

Ideal lattice

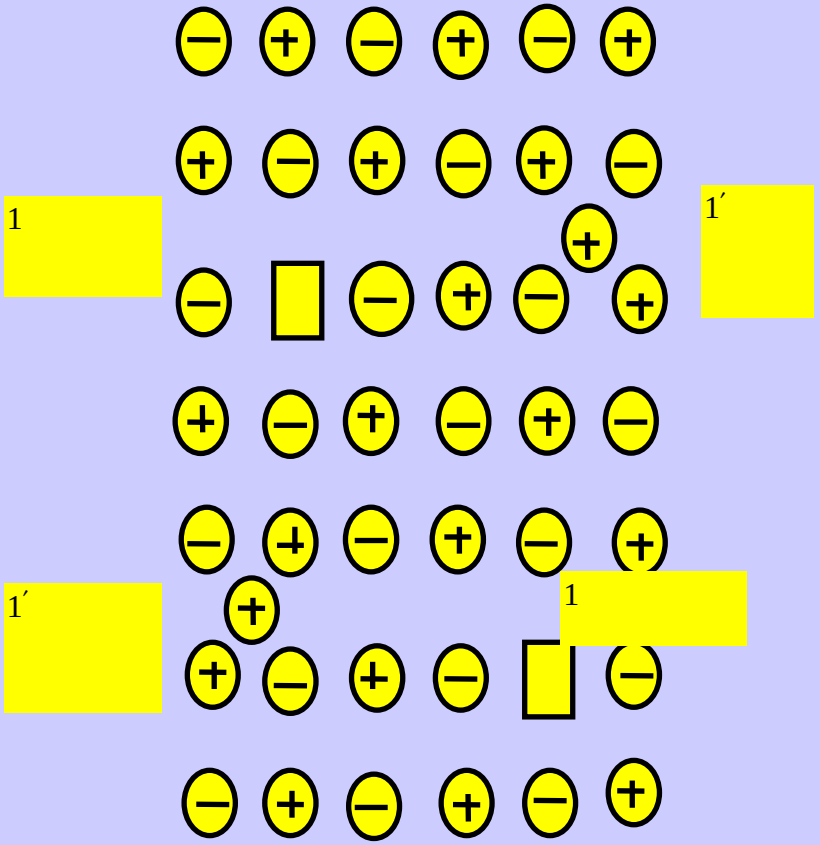


Point Frenkel –type defects

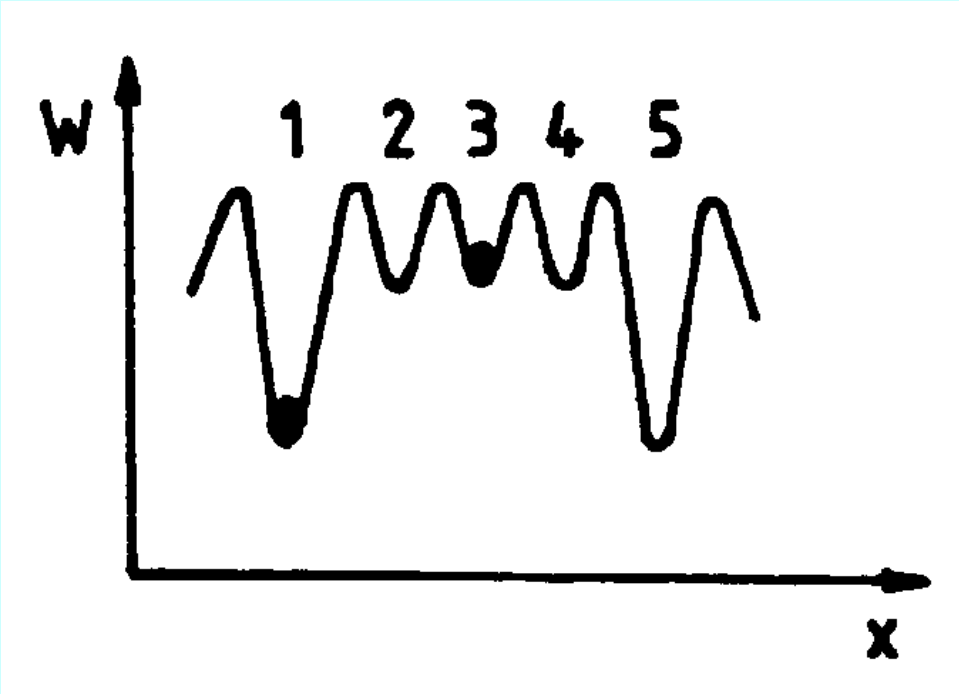


The energy relief of of ions in the lattice with the point Frenkel –type defects

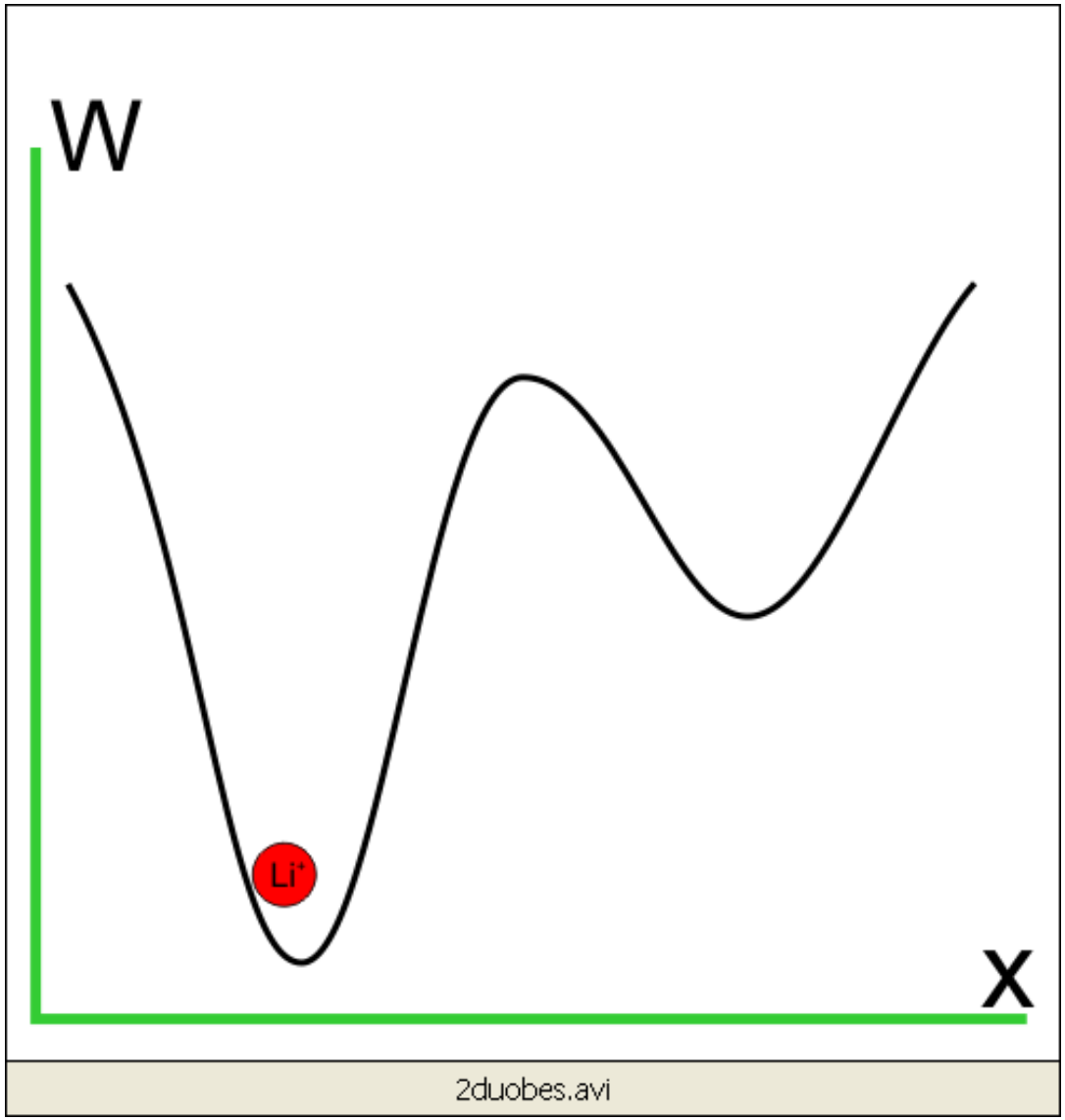
W
Li+
X
2duobes.avi

# Point Frenkel - type defect

$$N_j = N_v$$

$$F = N_F \cdot G_F - T \cdot S$$

$$G_F = H_F - T \cdot S_F$$

$$P_1 = \frac{N'!}{(N' - N_F)!N_F!}$$

$$P_2 = \frac{N!}{(N - N_F)!N_F!}$$

$$S = k \ln P \quad P = P_1 \cdot P_2$$

$$S = k(\ln P_1 + \ln P_2) = k \ln\left\{\frac{N'!}{(N' - N_F)!N_F!} \cdot \frac{N!}{(N - N_F)!N_F!}\right\} \qquad 1 << N_F << N, N'$$

$$\ln x! \approx x \ln x - x$$

$$k = 1{,}38 \cdot 10^{-23}\ J \cdot K^{-1}$$

$$\ln = \frac{N'!}{(N' - N_F)!N_F!} = \ln(N' - N_F)! - \ln N_F! =$$

$$= N' \ln N' - N' - (N' - N_F)\ln(N' - N_F) + (N' - N_F) - N_F \ln N_F + N_F =$$

$$= N' \ln N' - N' \ln(N' - N_F) + N_F \ln(N' - N_F) - N_F \ln N_F$$

$$\ln = \frac{N!}{(N - N_F)!N_F!} = N \ln N - N \ln(N - N_F) +$$

$$+ N_F \ln(N - N_F) - N_F \ln N_F; \quad \left(\frac{\partial F}{\partial N_F}\right) = 0$$

$$\frac{S}{k} = N \ln N - N' \ln N' - 2N_F \ln N_F -$$

$$- (N' - N_F)\ln(N' - N_F) - (N - N_F)\ln(N - N_F)$$

$$-\frac{G_F}{kT} = 2 \ln N_F - \ln(N - N_F) - \ln(N' - N_F)$$

$$N_F =<< N, N'$$

$$N_F^2 = (N - N_F)(N' - N_F)\exp\left(-\frac{G_F}{kT}\right)$$

$$N_F^2 = NN' \exp\left(-\frac{G_F}{kT}\right)$$

$$N_F = \sqrt{NN'} \exp\left(-\frac{G_F}{2kT}\right)$$

N'-j.tarpmazgiuose;

N-j.mazguose;

$P_1$-j.pasiskirstimo tikimybe;

$P_2$-vakansiju pasiskirstymo tikimybe;

$S_F = \Delta Q/T$; $H_F = U + pV$.

Stirlingo formulė

$N_j$-concentration of ions

$N_v$-concentration of vacancies

$N_F$-concentr.of p.Frenkel def.

F-free energy of lattice

$G_F$-Gibbs energy

S-entrophy $S = \delta Q/T$

$H_F$-enthalpy $H = TS + pV$

$P_1, P_2$-probabilities

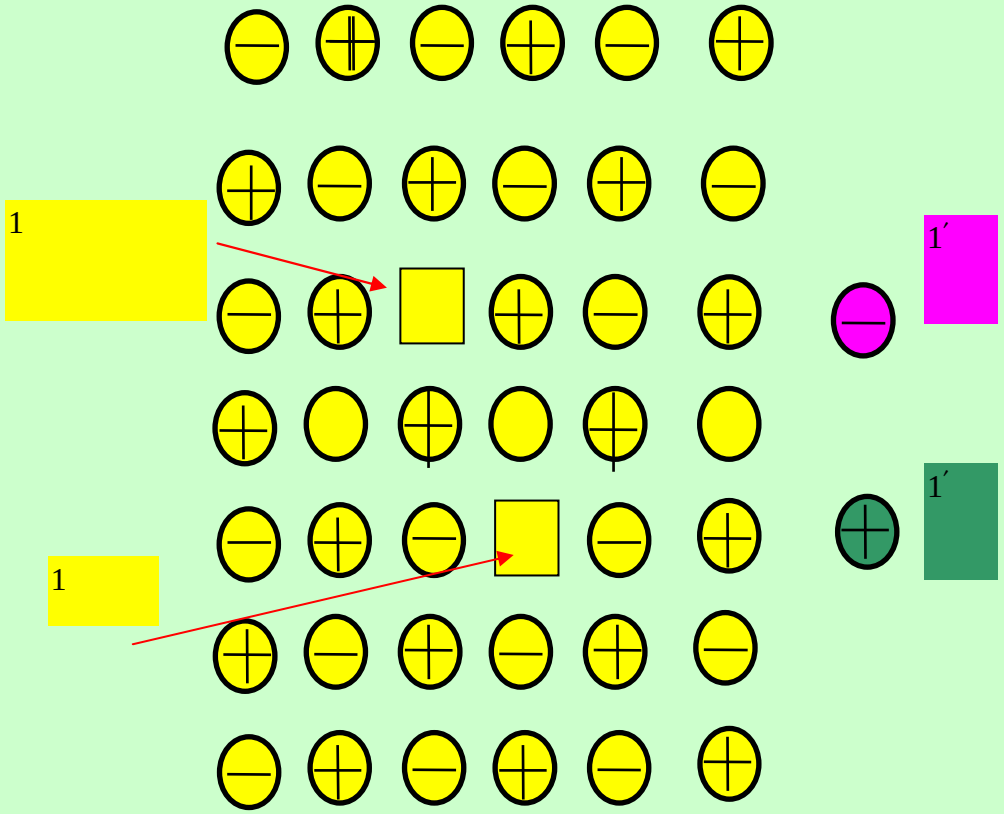


Point Schottky-type defects

# Point Schottky-type defect

$$F = N_s \cdot G_s - T \cdot S$$

$$G_s = H_s - T \cdot S_s$$

$$P = \frac{N'!}{(N - N_s)!\,N_s!}$$

$$S_s = k \ln P = k \ln \frac{N!}{(N - N_s)!\,N_s!}$$

$$G_S = T \frac{\partial S_S}{\partial N_S}$$

$$\frac{\partial S_S}{\partial N_S} = k \ln \frac{N_S}{N_S}$$

$$\frac{G_S}{k \cdot T} = \ln \frac{N}{N_S}$$

$$N_S = N \exp\left(-\frac{G_S}{k \cdot T}\right)$$

F-free energy of the lattice

$N_s$-concentr. of p.Schottky defects

N-concentration of the ions inttice

T-temperature

P-probability

$G_s$-Gibbs energy

## The substitution of $M^{3+}$ and $M^{2+}$ ions in $LiTi_2(PO_4)_3$ solid electrolytes

The values of the ionic radius are: $Ti^{4+}=0.6$, $Sc^{3+}=0.81$, $Fe^{3+}=0.76$, $Y^{3+}=0.93$, $Al^{3+}=0.5$, $Ge^{4+}=0.53$, $Cr^{3+}=0.69$, $Mg^{2+}=0.65$ Å .

The compounds at room temperature belongs to the rhobohedral symmetry
(.S.G. $R\bar{3}c$) Z=6

The substitution $Ti^{4+} \rightarrow M^{3+} + Li^{+}$ realize in the compounds
$Li_{1+x}M_xTi_{2-x}(PO_4)_3$ Where M = Sc, Al, Fe, Y, La, x= 0.3.

The substitution $Ge^{4+} \rightarrow M^{3+} + Li^{+}$ realize in the compounds
$Li_{1+x}Ge_{2-x}M_x(PO_4)_3$ Where $M_x = Al_{0.5}, Cr_{0.3}$.

The substitution $Ti^{4+} \rightarrow M^{2+} + 2Li^{+}$ realize in the compounds
$Li_{1+2x}M_xTi_{2-x}(PO_4)_3$ Where $M_x = Mg_{0.3}$.

**Synthesis conditions of the**
**$Li_{1+x}M_xTi_{2-x}(PO_4)_3$ (where M=Sc, Al, Fe, Y; x=0.3) compounds by a solid phase reaction**

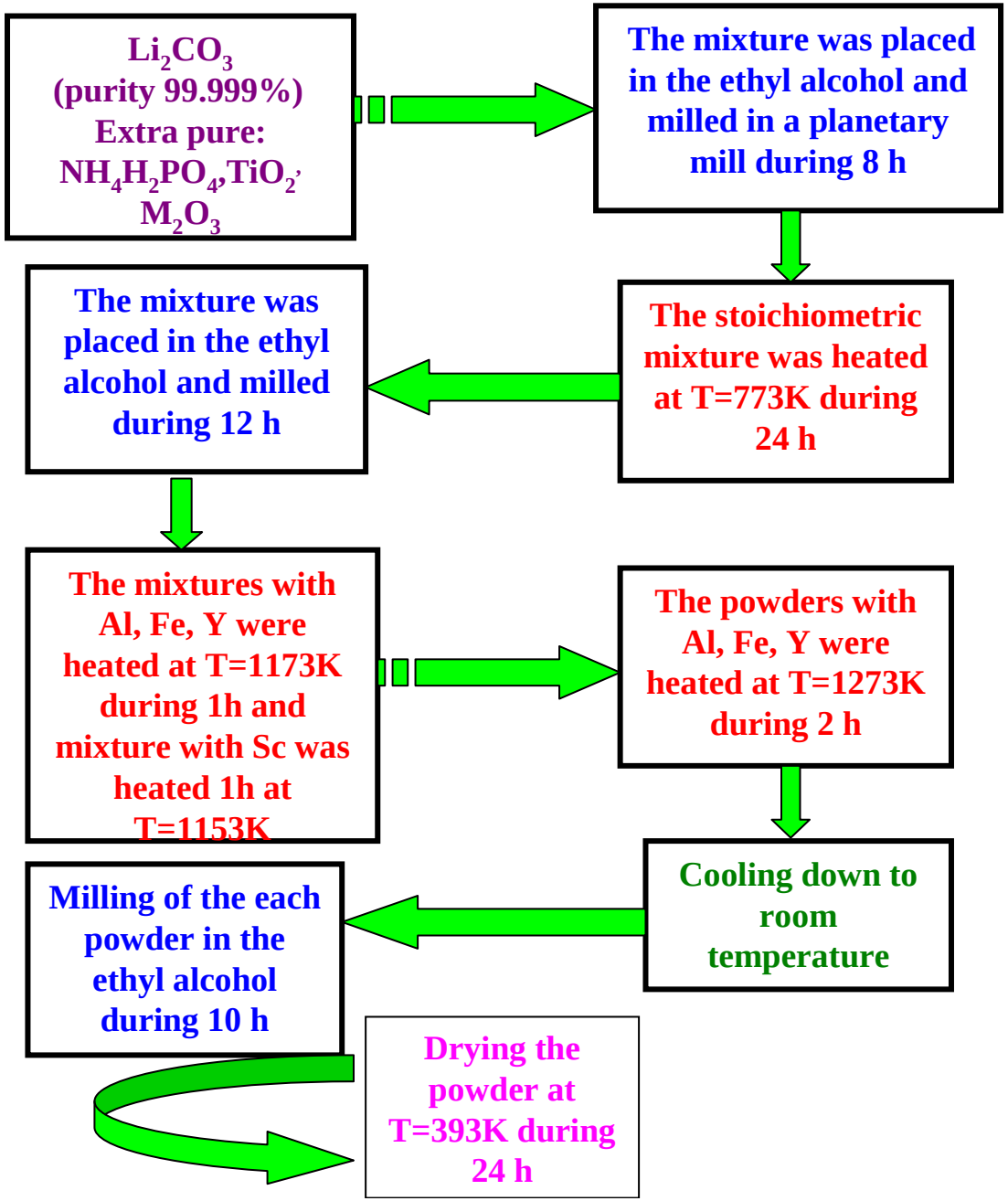

**Sintering of the $Li_{1+x}M_x Ti_{2-x}(PO_4)_3$ (where M=Sc, Al, Fe, Y; x=0.3) ceramics**

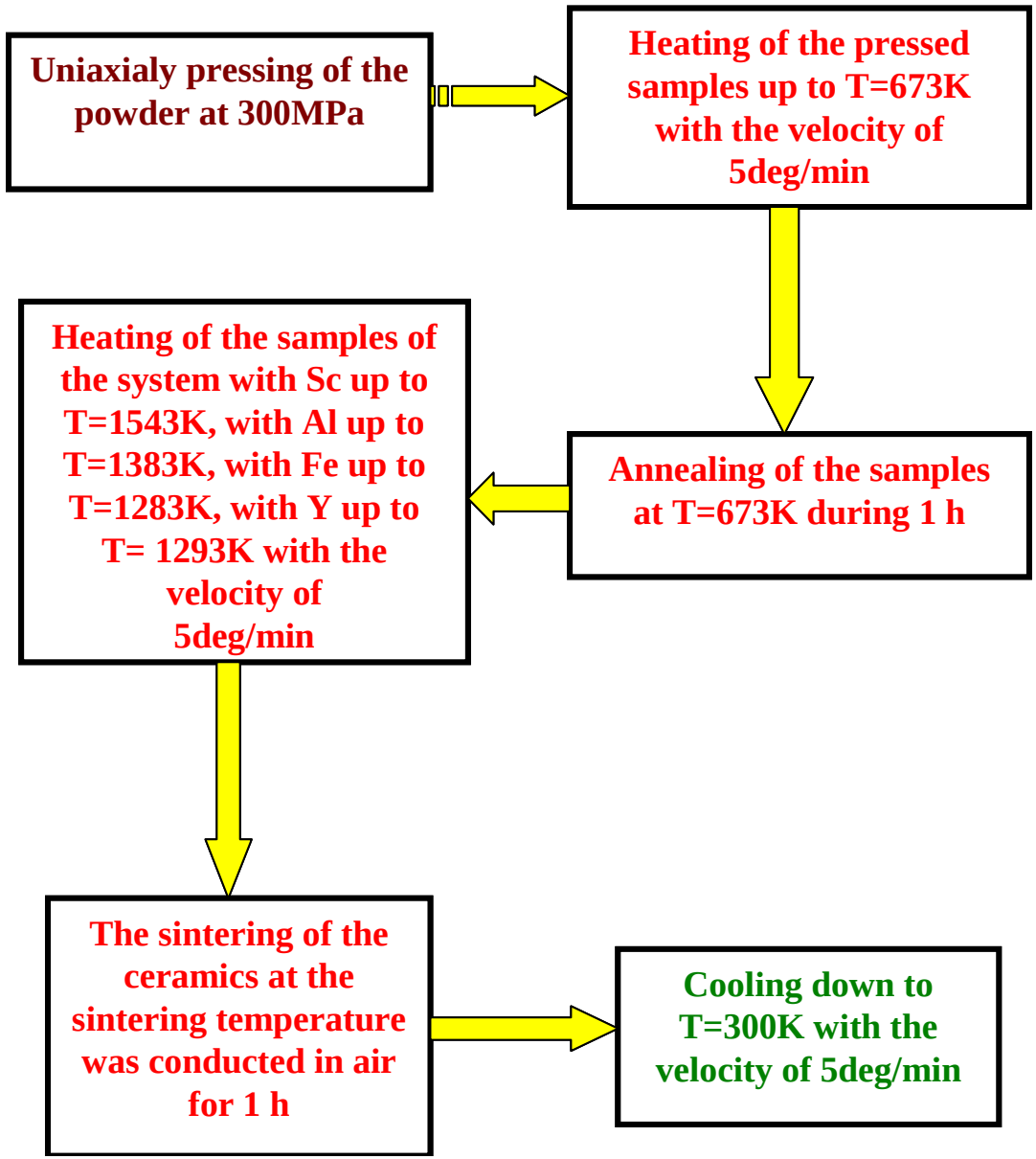

In 1938, Stefan Brunauer, Hugh Emmett and Edward Teller published an article about the BET theory in a journal for the first time; “BET” consists of the first initials of their family names.  [BET ($m^2/g$)].

10 μm

YSZ, GDC, SDC composition, $S_{BET}$ of the powder theoretical and relative densities of the ceramics.

| Composition | $S_{BET}$, $m^2/g$ | $D_{theoretical}$, $g/cm^3$ | *d*, % |
|---|---|---|---|
| $Gd_{0.2}Ce_{0.8}O_{1.9}$ | 220 | 7.24[3] | 95.0 |
| $Sm_{0.2}Ce_{0.8}O_{1.9}$ | 212 | 7.15[1] | 94.0 |
| $Sm_{0.15}Ce_{0.85}O_{2-\delta}$ | 195 | 7.22[5] | 94.0 |
| $Sm_{0.15}Ce_{0.85}O_{1.925}$ | 203 | - | 94.0 |
| $Sm_{0.15}Ce_{0.85}O_{1.925}$ | 8 | - | 92.0 |
| $Gd_{0.1}Ce_{0.9}O_{1.95}$ | 6.44 | 7.21[2] | 97.0 |
| $Gd_{0.1}Ce_{0.9}O_{2-\delta}$ | 201 | - | 95.0 |
| 92 mol% $ZrO_2$ 8 mol% $Y_2O_3$ | 1.67 | 5.96[4] | 97.0 |
| 92 mol% $ZrO_2$ 8 mol% $Y_2O_3$ | 12.4 | - | 95.0 |

**1.** H.B.Li et al.Acta Mater.54(2006)721; **2.** K.Huang et al.J.Amer.Ceram.Soc.81(1998)357;**3.**G.Chiadeli et al.Sol.State Ioncs, 176(2005)1505; **4.** H.Liu et al.Mat. And Design, 31(2010)2972; **5.** C.Jiang et al. Power Sources, 165(2007)134.

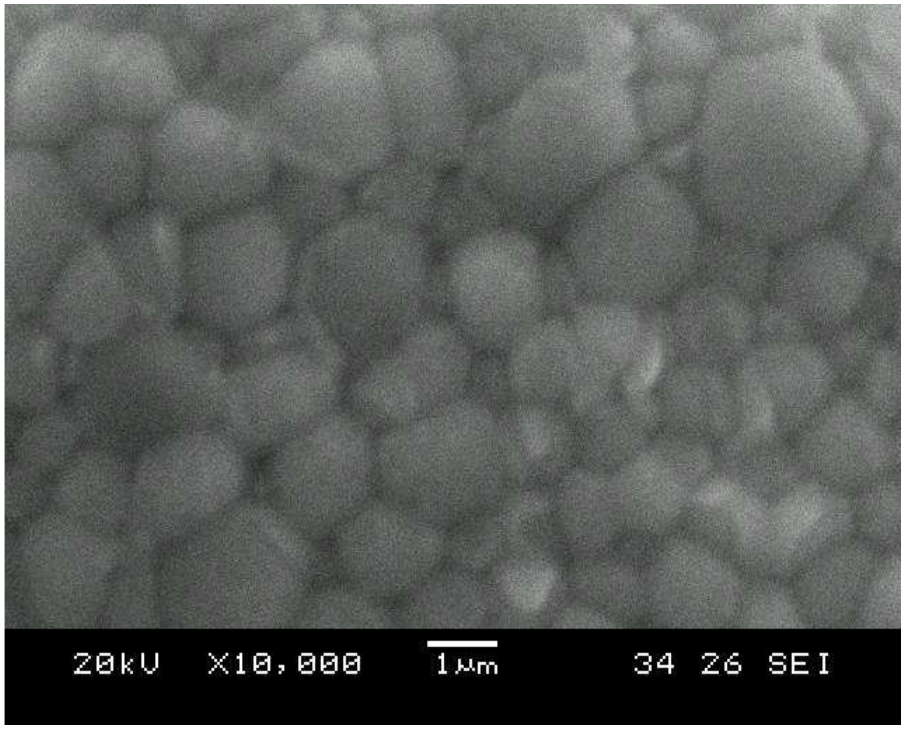


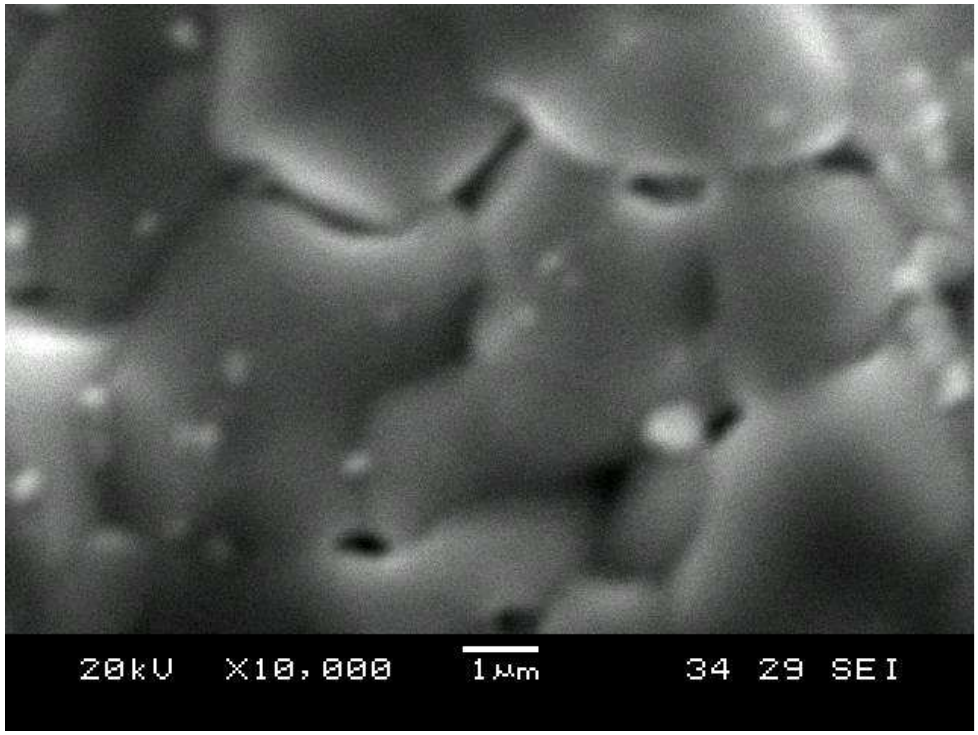


a) b)

**SEM images of $Ce_{0.9}Gd_{0.1}O_{1.95}$ ceramics sintered from powder with $S_{BET}$ = 158.03 $m^2/g$ (a) and $S_{BET}$ = 6.44 $m^2/g$ (b)**

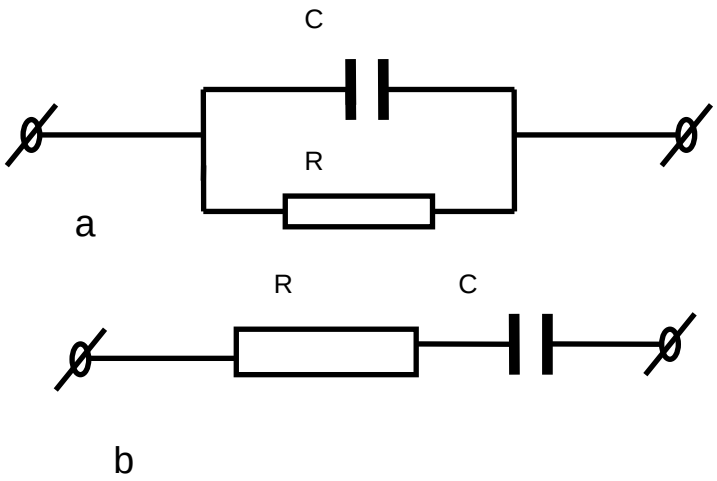


Vektrinės diag-ra-mos: sro-vių,
Lygiagrečios RC grandinės atveju

$$\mathrm{tg}\delta = \frac{j_a}{j_r} = \frac{\varepsilon''}{\varepsilon'} = \frac{1}{\omega R C},$$

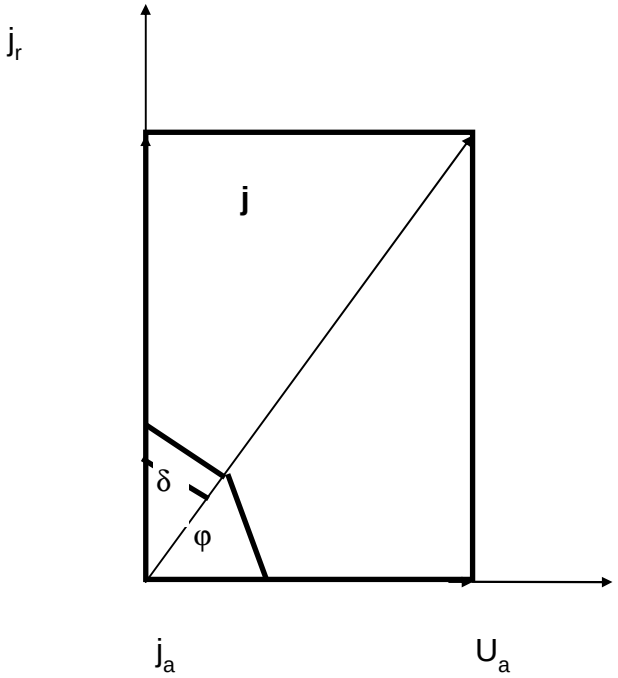


a)

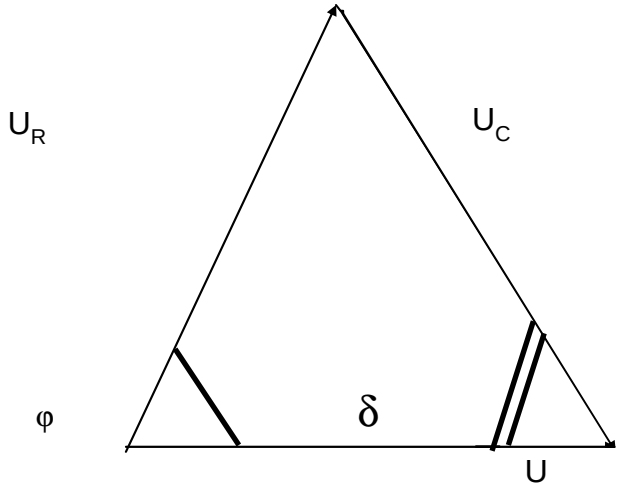


b)

# Nuoseklios grandinės

$$\mathrm{tg}\delta = \frac{u_R}{u_C} = \omega R C.$$

$$\varepsilon'' = \frac{\sigma}{\varepsilon_0 \omega} + \frac{\left(\varepsilon'_m - \varepsilon'_{j\infty}\right)\omega\tau'}{1+\left(\omega\tau'\right)^2}$$

$$\varepsilon' = \varepsilon'_{j\infty} + \frac{\varepsilon'_m - \varepsilon'_{j\infty}}{1+\left(\omega\tau'\right)^2}.$$

Pastarosios lygtys yra vadinamos Debajaus lygtimis. Joniniuose ir superjoniniuose kristaluose, kuriuose dominuoja vienarūšiai joniniai migrato-riai, turintys tą patį relaksacijos laiką

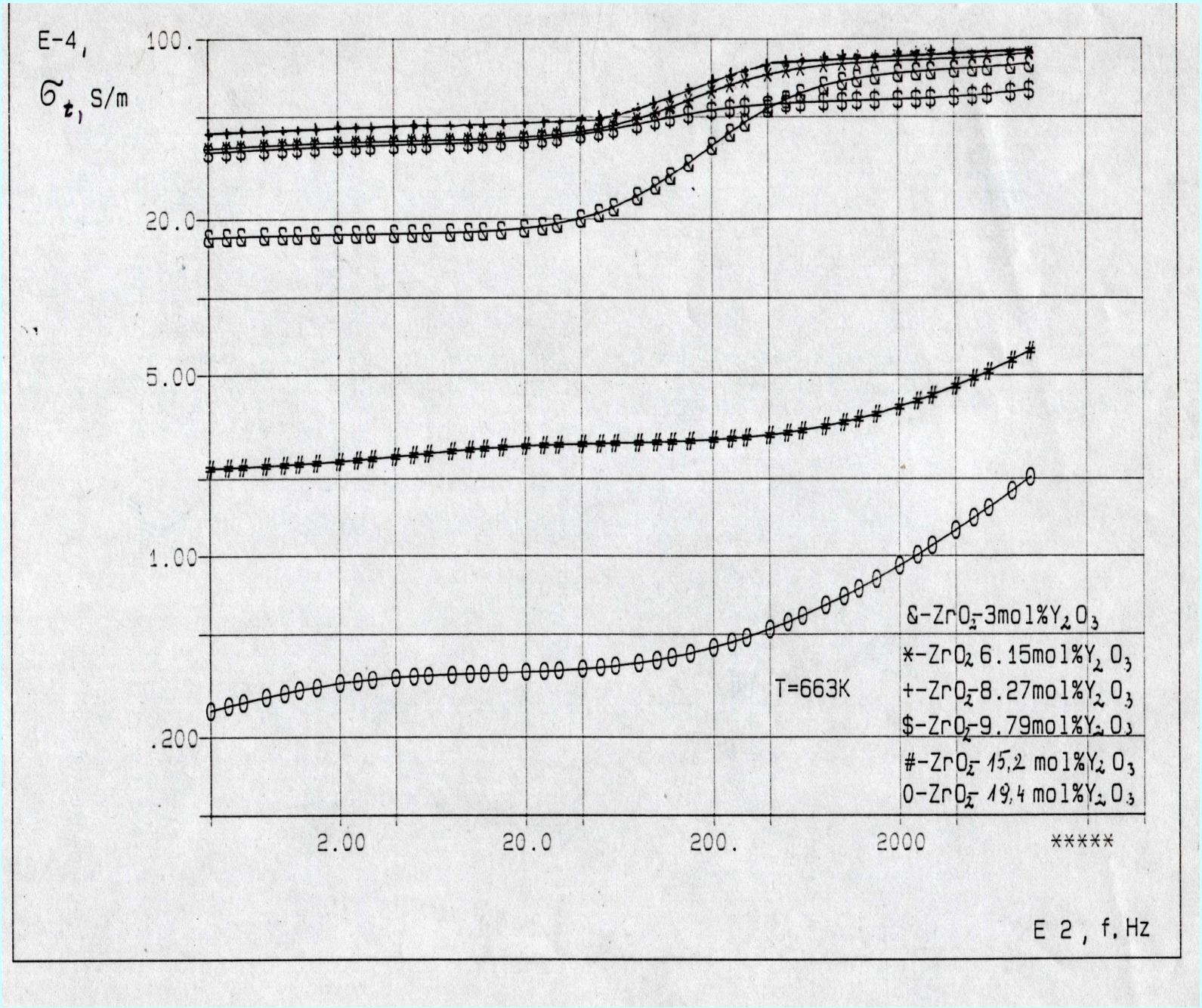
E-4,
σt, S/m
100.
20.0
5.00
1.00
.200
2.00
20.0
200.
2000
*****
E 2 , f, Hz
T=663K
&-ZrO2-3mol%Y2O3
*-ZrO2 6.15mol%Y2O3
+-ZrO2-8.27mol%Y2O3
$-ZrO2-9.79mol%Y2O3
#-ZrO2- 15,2 mol%Y2O3
0-ZrO2- 19,4 mol%Y2O3

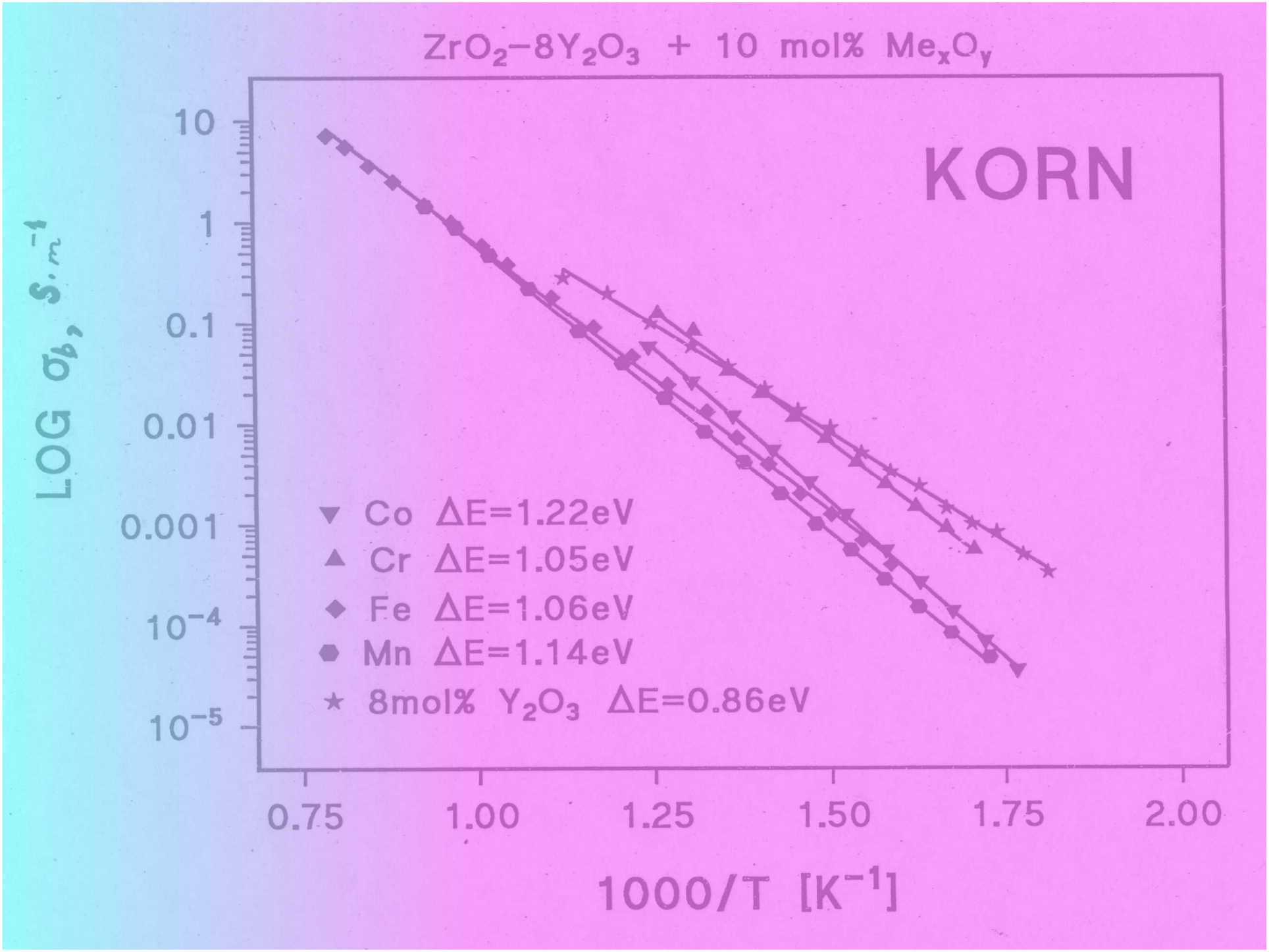
$ZrO_2$–8$Y_2O_3$ + 10 mol% $Me_xO_y$
KORN
LOG $\sigma_b$, $S.m^{-1}$
10
1
0.1
0.01
0.001
$10^{-4}$
$10^{-5}$
▼ Co ΔE=1.22eV
▲ Cr ΔE=1.05eV
◆ Fe ΔE=1.06eV
⬢ Mn ΔE=1.14eV
★ 8mol% $Y_2O_3$ ΔE=0.86eV
0.75
1.00
1.25
1.50
1.75
2.00
1000/T [$K^{-1}$]

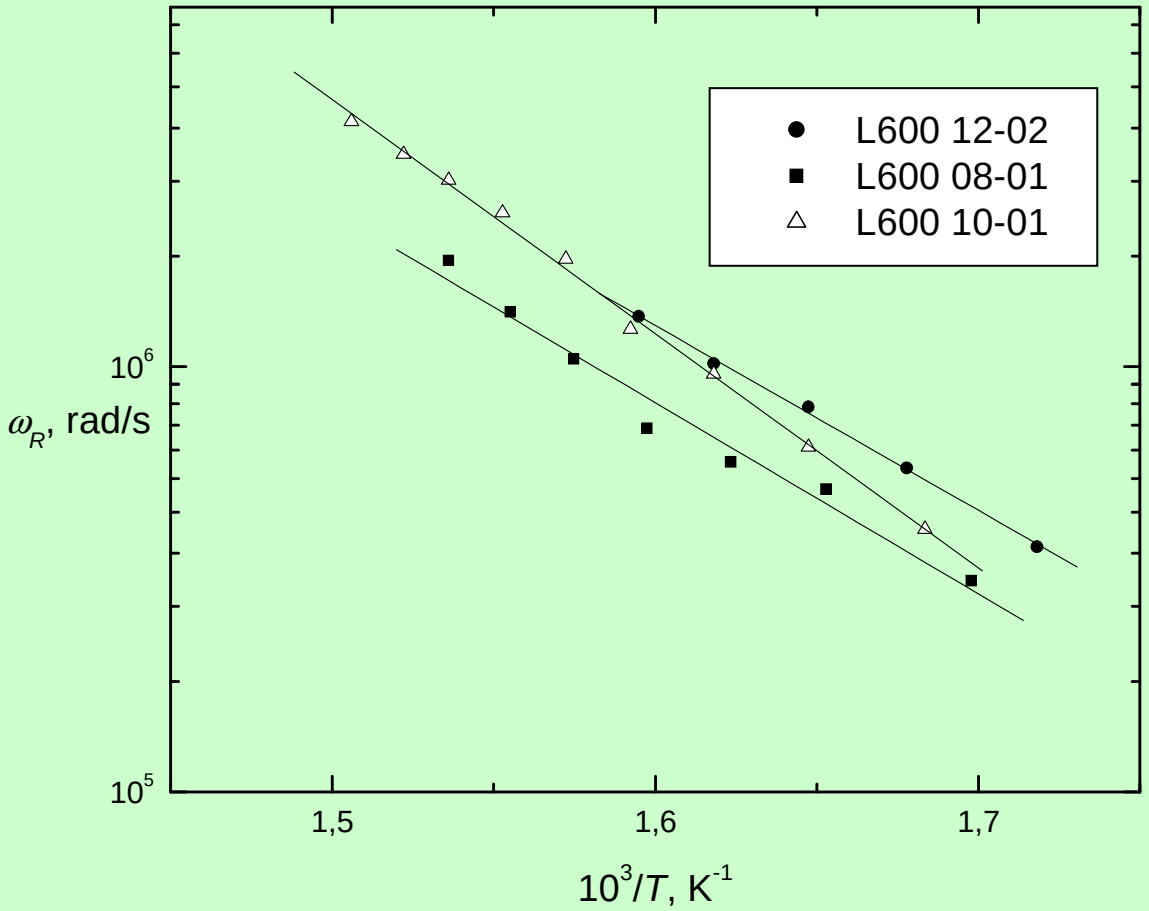


**Temperature dependences of the relaxation frequency of the YSZ thin films deposited on alloy-600 substrate**

The frequency of the relaxation dispersion increase with temperature according to formula

$$f_b = f_0 \exp\left(-\frac{\Delta E_f}{kT}\right),$$

where $f_0$ is frequency related to the lattice vibration. The ionic conductivity of the bulk is the product of the volume concentration of mobile $Li^+$ ions N, their electric mobility $\mu$ and the electric charge q:

$$\sigma_b = \mu N q .$$

$$\sigma_b = \left[N_0 \exp\left(-\frac{\Delta E_N}{kT}\right)\right] \cdot \left[\frac{C}{kT} \exp\left(-\frac{\Delta E_\mu}{kT}\right)\right] q ,$$

$$\Delta E_N + \Delta E_\mu = \Delta E_b .$$

According to the Nernst-Einstain relation, the diffusion coefficient of mobile ions $D = \frac{\mu kT}{q}$ and

exponentially increase with temperature according formula $D = D_0 \exp(-\Delta E_D / kT)$.

That means that the activation energy of $Li^+$ ion diffusion $\Delta E_D$ and migration $\Delta E_\mu$ should be equal

$$\Delta E_D = \Delta E_\mu .$$

According to model of thermally activated ion jumps, which is realized in solid electrolytes, the lattice diffusion coefficient of mobile ions are related to the mean jump frequency $\omega_j$ by the expression:

$$D = \chi \gamma l^2 \omega_j ,$$

where $\omega_j = 2\pi f_b$ is the angular frequency, $\chi = 1/4$ is the geometric factor for two-dimensional conductivity path in the rhombohedral site symmetry, $l^2$ is the mean square jump and $\gamma$ is the correlation factor, which depends on the definition and probability population of jump vectors. Since we have found that the activation energy the $\sigma_b$ of the materials is equal to the activation energy of the $f_b$, which can be attributed to the migration of $Li^+$ ions in the bulk of the ceramic samples, the concentration of charge carriers remains constant with temperature.

$$\mathcal{E} = \frac{RT}{4F} \ln \frac{P_{O_2}'}{P_{O_2}''} \; ; \quad F = 9.6487 \cdot 10^7 \; C/kg$$

$$R = 8.3143 \cdot 10^3 \; J/k.kmol$$

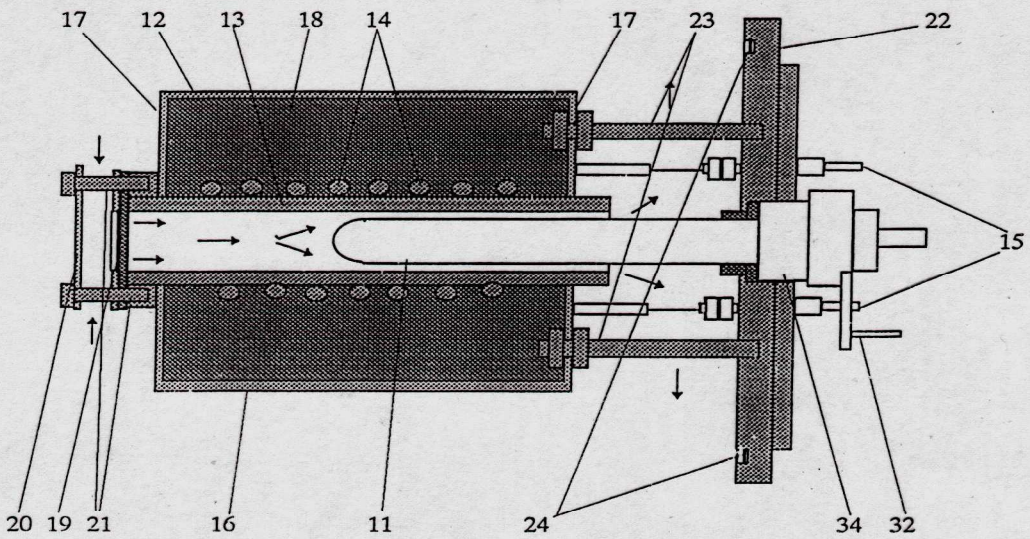


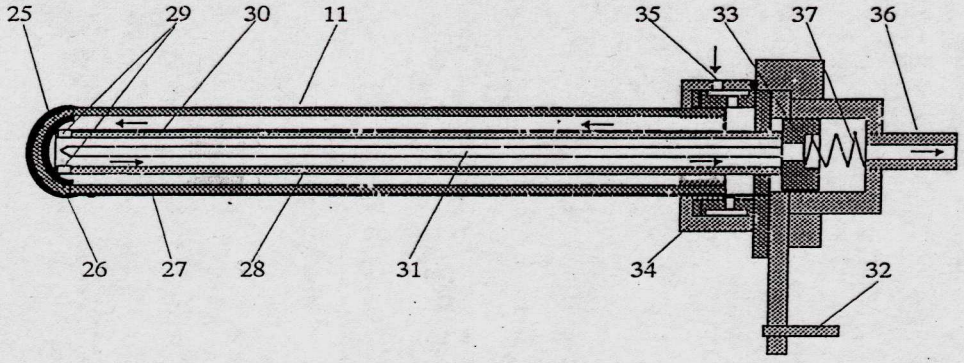

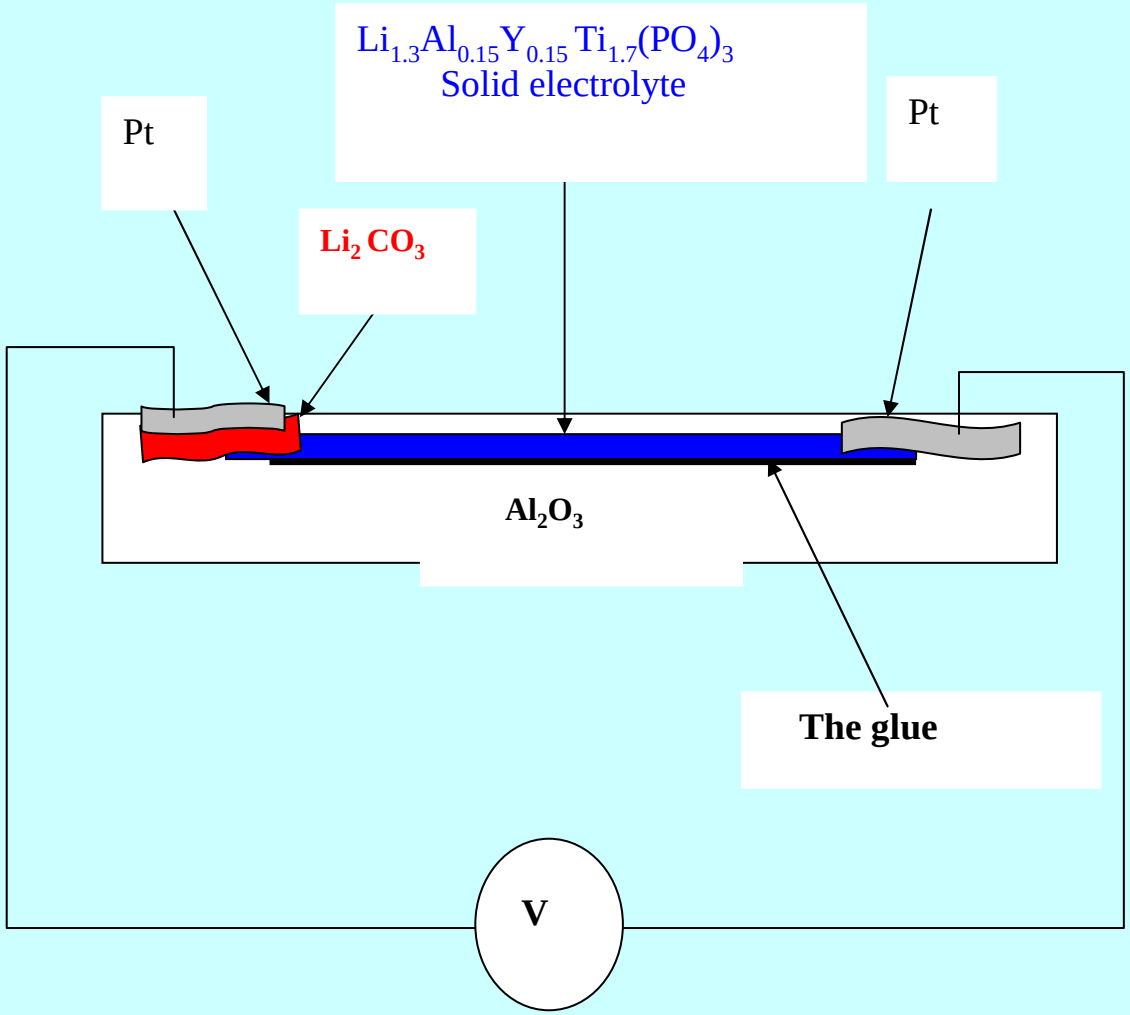


# $CO_2$ dujų jutiklio struktūrinė schema

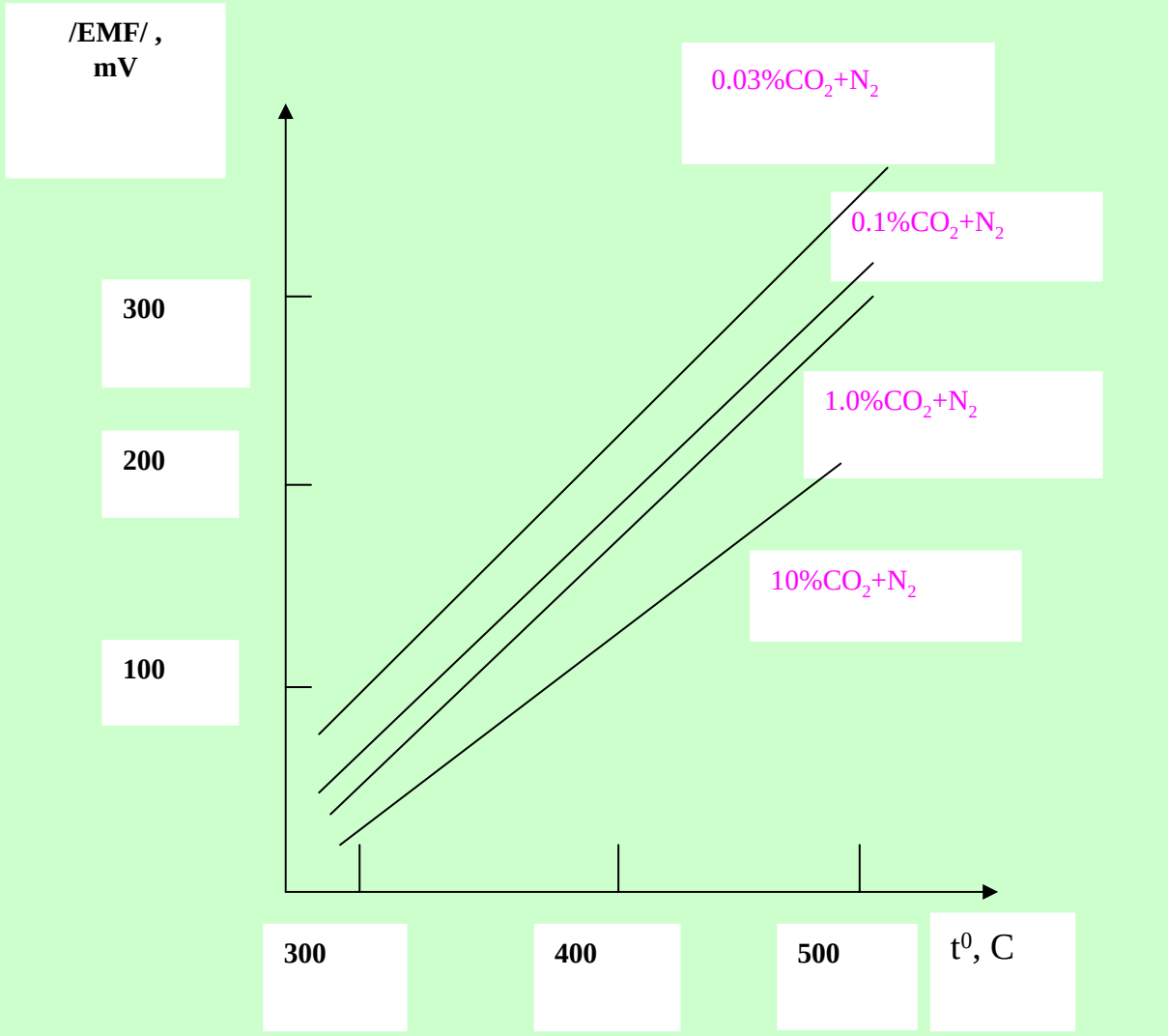


.$CO_2$ dujų jutiklio E-P-T charakteristikos

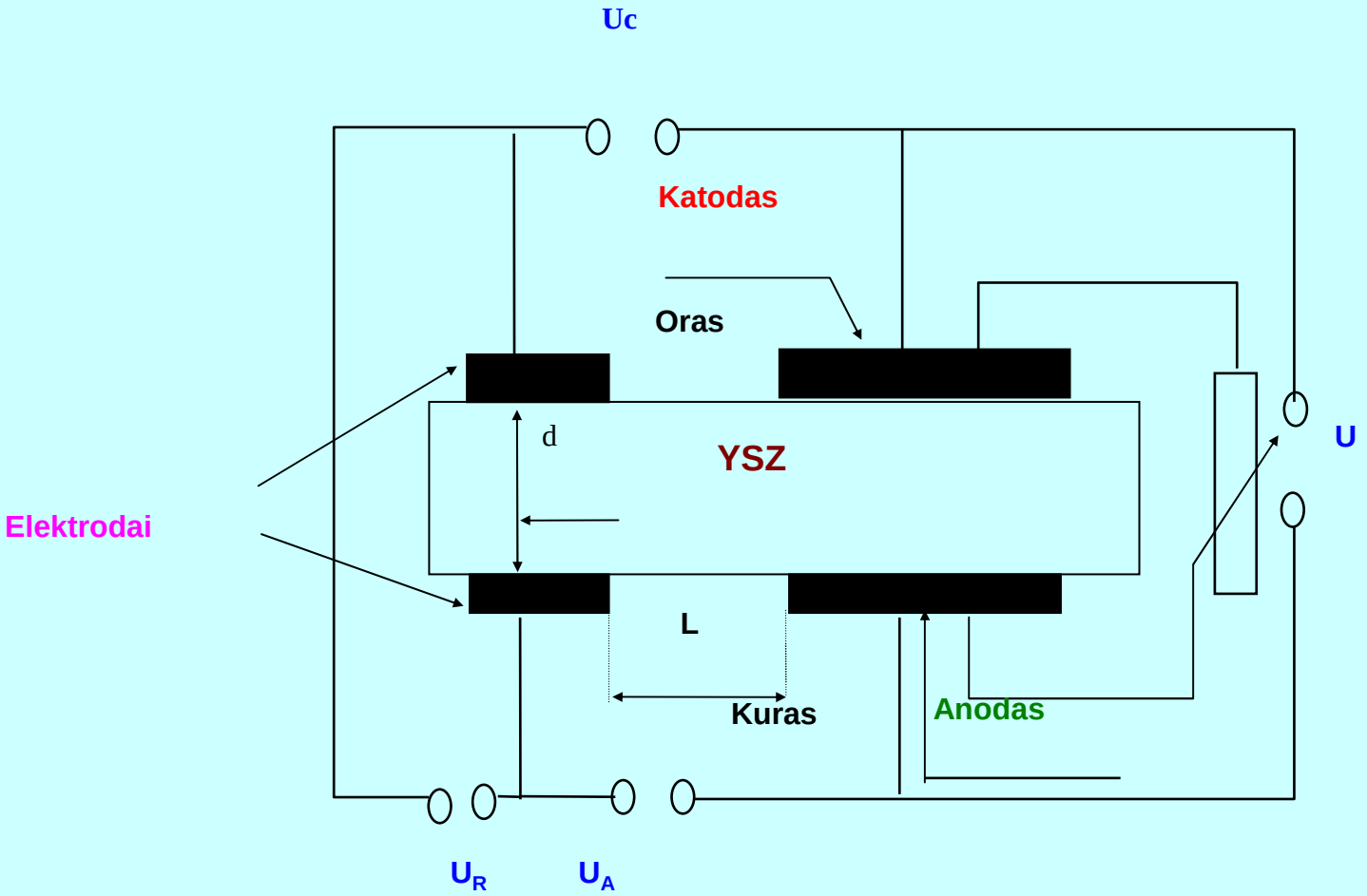


**Kietojo elektrolito kuro gardelės struktūrinė schema**

## JAV SOFC PROGRAMOJE DIRBA:

1. NACIONALINIS KOMERCINIS STANDARTŲ IR TECHNOLOGIJŲ DEPARTAMENTAS
2. FEDERALINIS ENERGETIKOS TECHNOLOGIJŲ CENTRAS
3. GYNYBOS DEPARTAMENTAS
4. DUJŲ TYRIMO INSTITUTAS
5. ELEKTRINIŲ IŠTEKLIŲ TYRIMO INSTITUTAS
6. BERKLIO LAWRENCO LABORATORIJA
7. KALIFORNIJOS UNIVERSITETAS

## VISŲ MINĖTŲJŲ ORGANIZACIJŲ ŠIUOS DARBUS FINANSUOJA:

1. CERAMATEC
2. ZTEK
3. TECHNOLOGIJŲ VALDYBOS
4. GIMININGŲJŲ SIGNALŲ AEROVISATOS KORPORACIJA

## AUSTRALIJOJE SOFC GAMINAMI KERAMIKINIŲ KURO GARDELIŲ LABORATORIJOJE

## EUROPOJE:

## DIRBAMA ŠVEICARIJOJE, ANGLIJOJE, VOKIETIJOJE, PRANCŪZIJOJE, DANIJOJE

## State-of-the-art SOFC

Unfortunately, the dominant SOFC developers aim at stationary applications. Such ceramic solutions are indeed heavy, sluggish, expensive and fragile and must be operated at high temperatures. But totally different SOFCs are presently developed for mobile applications. The following results, **Table 1**, have recently been presented:

**Table 1** Recent results reported by distinguished SOFC laboratories

| Feature | Value | References |
|---|---|---|
| Power density at 800°C | 1.935 W / $cm^2$ | Berkeley Lawrence Lab. (2) |
| Stack power per volume | over 1 kW / L | Allied-Signal Aerospace (3) |
| Stack power per mass | over 1 kW / kg | Allied-Signal Aerospace (3) |
| Warm-up: to 800°C | 1 minute | Keele University (4) |
| or „to operating temperature" | 5 seconds | Keele University (5) |
| Cool-down, 1000 to 800°C | 31 hours | Univ. of California (6) |

Although these results come from different laboratories, they illustrate the potentials of advanced SOFC technology: planar, hybrid (metal-ceramic), bipolar designs with thin (5 to 10 µm) supported ceramic electrolytes and operating temperatures between 650°C and 800°C. Such light weight, compact SOFCs are under development for automotive applications. **Table 2** documents what can be expected in the near future:

**Table 2** Projected trends of development of SOFCs for transportation

| Features | Projections |
|---|---|
| Operating temperature | (550°C) 600°C to 800°C |
| Start-up (ambient to operating temp.) | less than 2 minutes |
| Stack power per volume | 2 kW / L |
| Stack power per mass | 2 kW / kg |
| Fuel | unleaded gasoline, diesel, Methanol |
| Reforming | integrated internal and in situ |
| Cooling | air, heat rejection by exhaust |
| Duty lifetime | 5,000 hours |

Šiluminė izoliacija

Kuro įvedimo anga

Oro įvedimoanga

SOFC tuščiaviduriai cilindrai

Vėsinimo kanalas

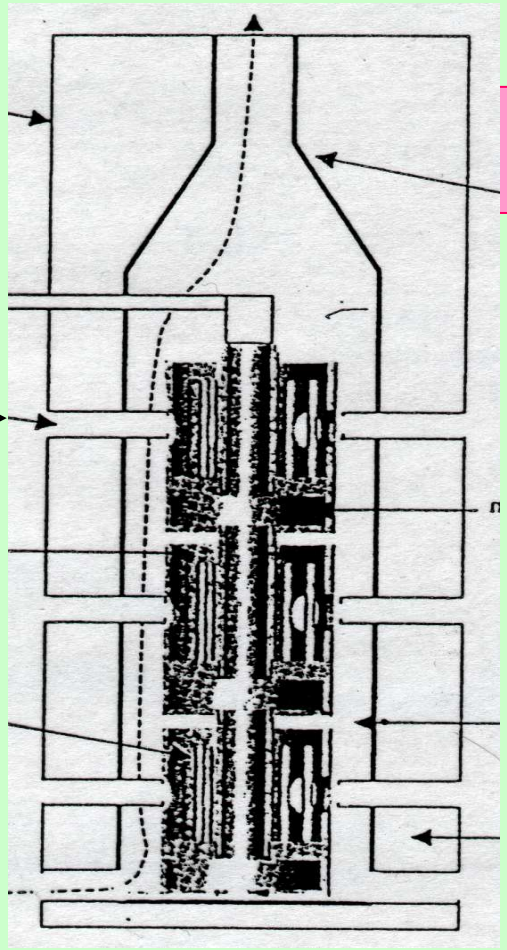

$H_2O$ garų išėjimo kanalo išorinė sienelė

H2O garų išėjimo kanalas

Vidinė izoliacija

# Cilindrinės formos SOFC modulis

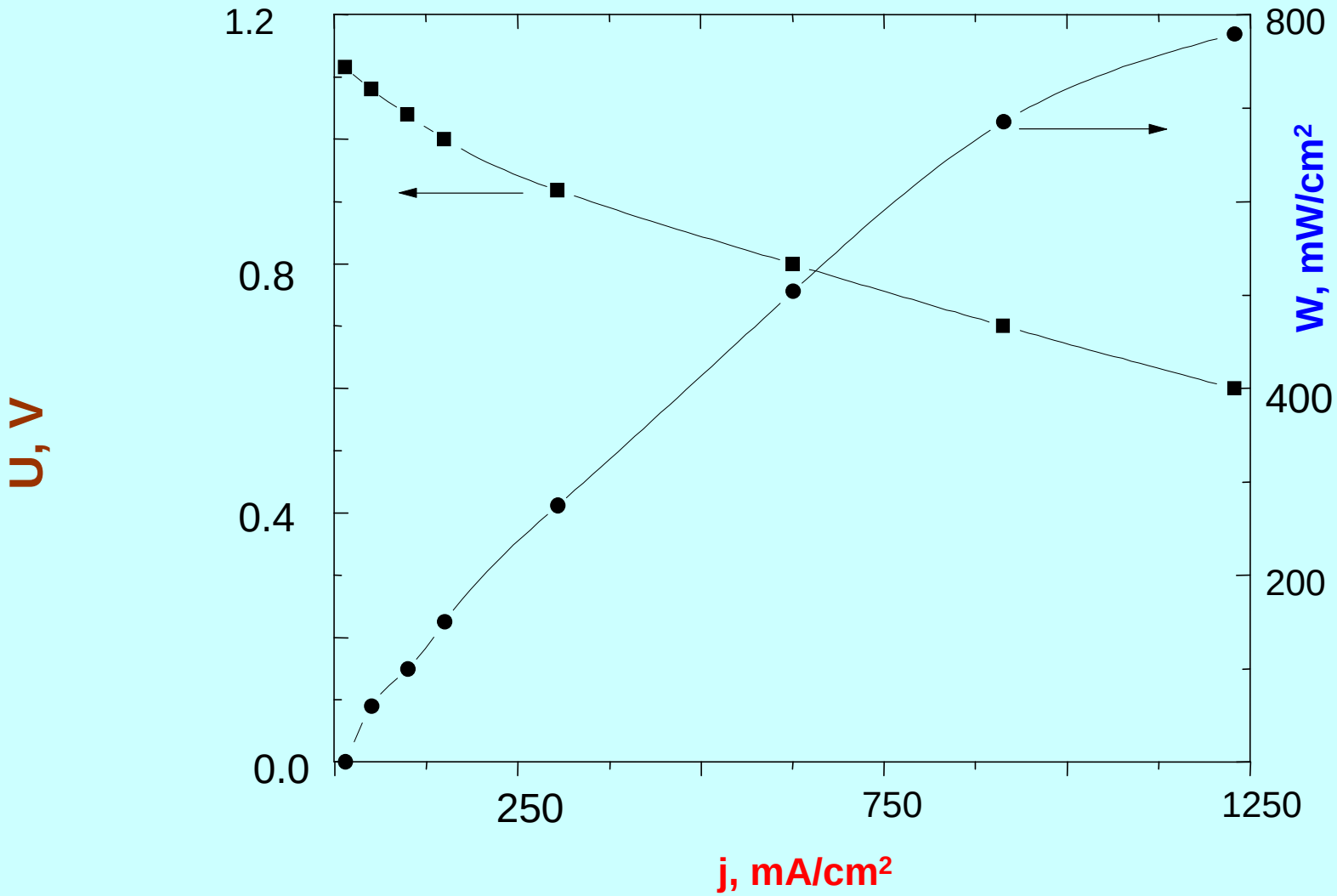


Storasluoksnio SOFC U – j – W charakteristikos

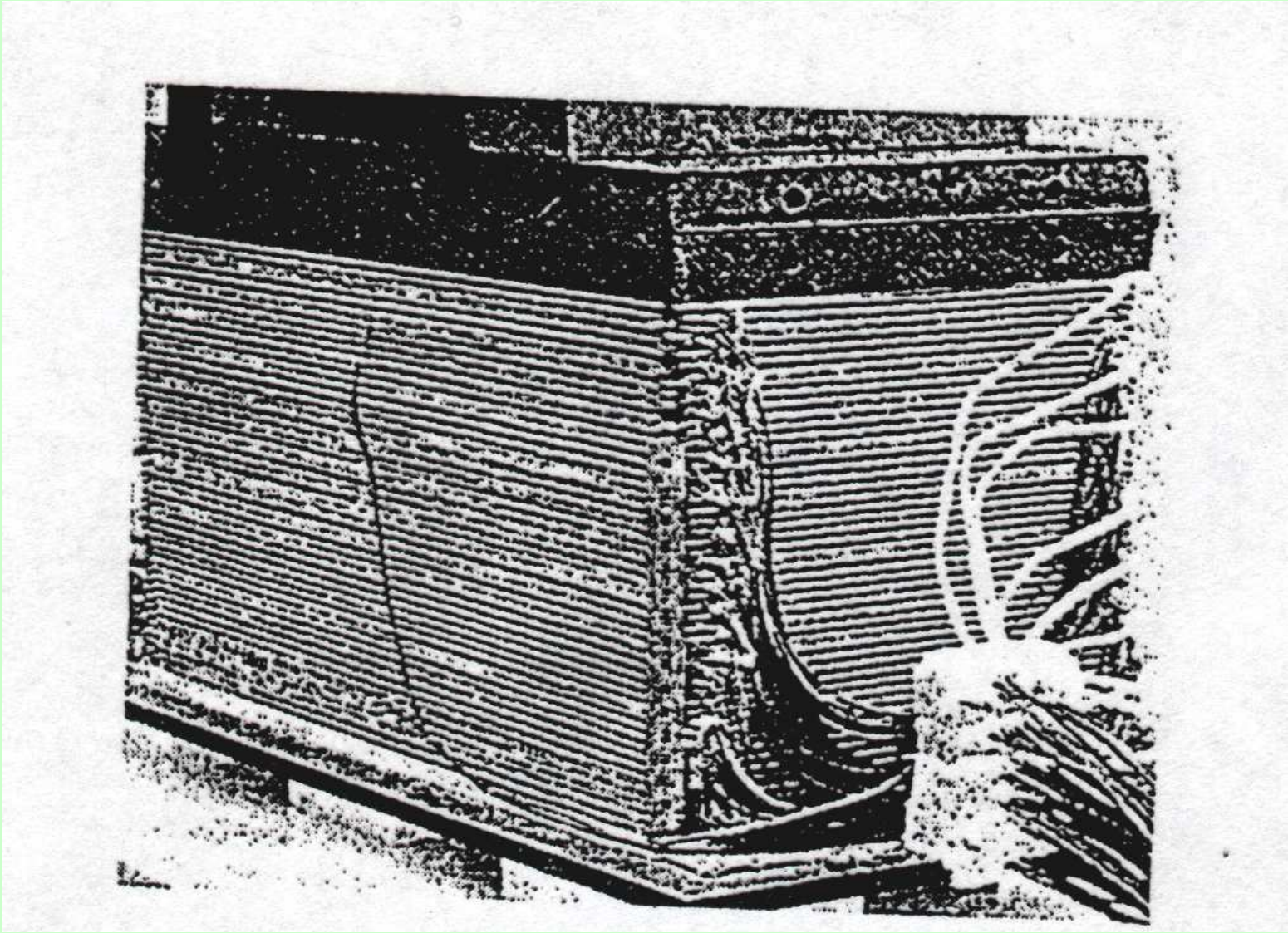

5kW SOFC modulis pagal S.P.S. Badwal ir K. Foger

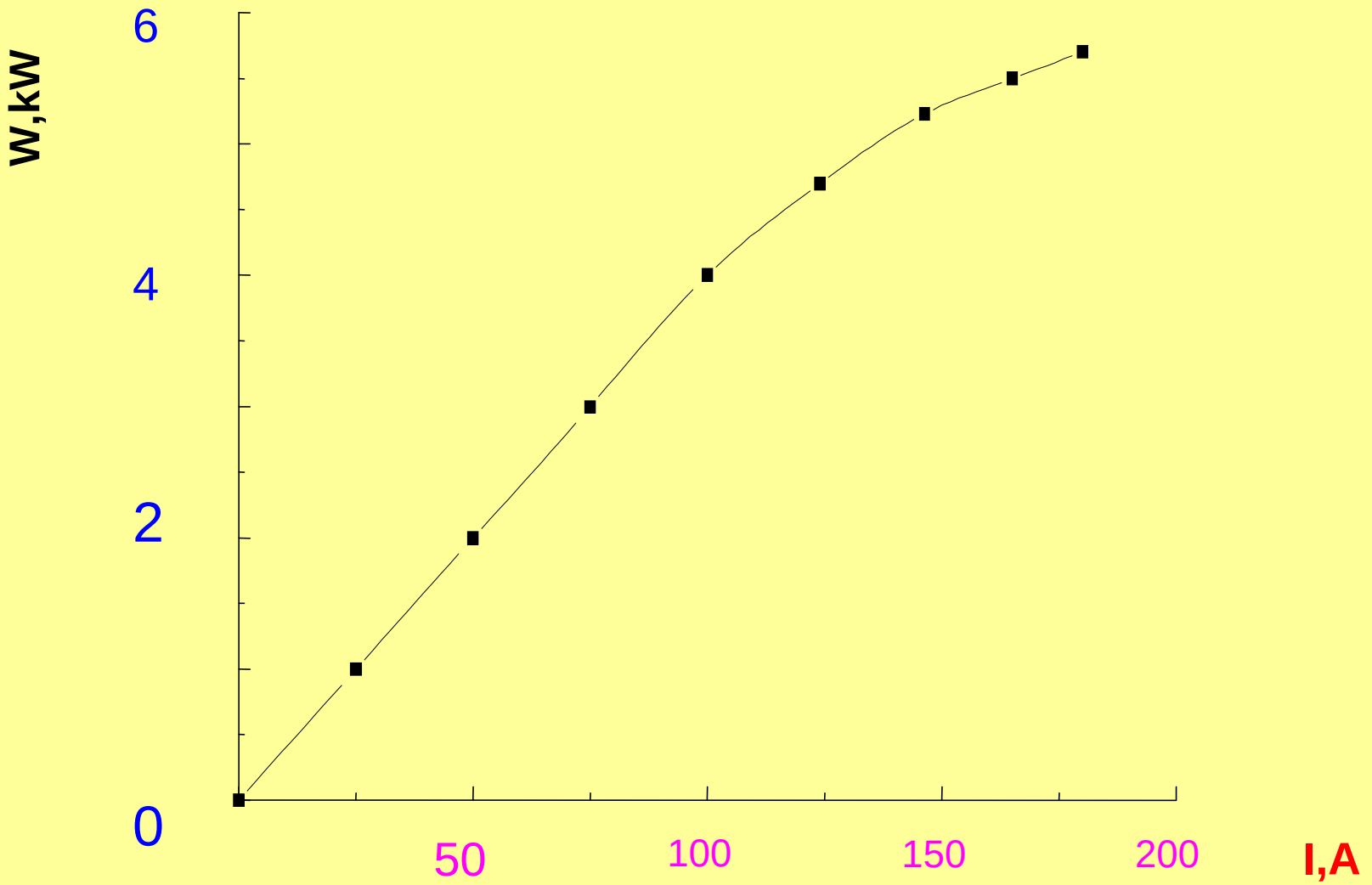


**SOFC W – I charakteristika 1203 K temperatūroje**

*The first approach: Thermodynamically stable mixed conducting composite*

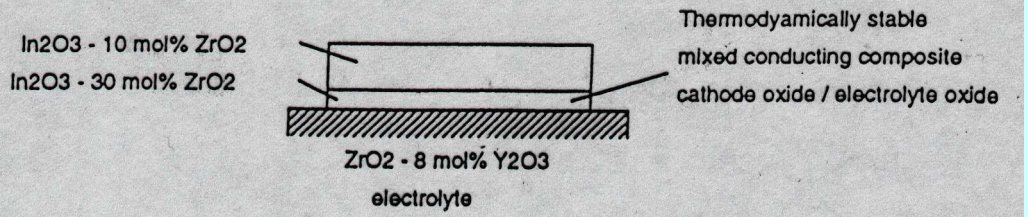


*The second approach: Multi-layer composite*

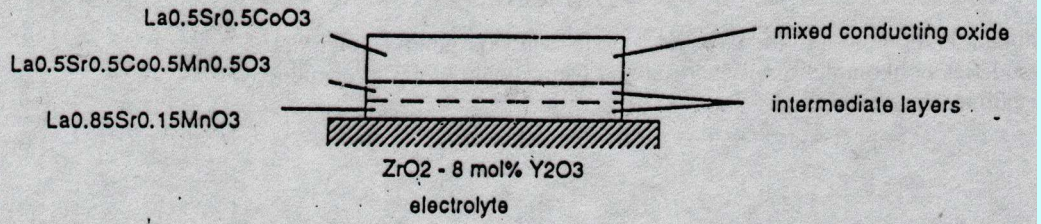


*The third approach: Concentration gradient cathode/electrolyte composite*

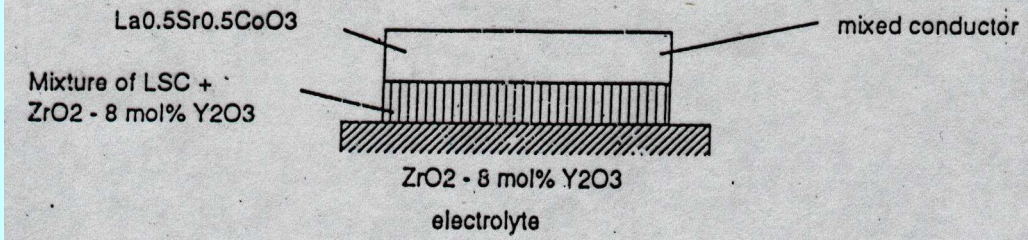

| | Electronic conductivity (S/m) | | | Ionic conductivity (S/m) | Thermal expansion coefficient ($10^{-6}.K^{-1}$) (R.T.-900°C) |
|---|---|---|---|---|---|
| | 950°C | 900°C | 800°C | | |
| $La_{0.85}Sr_{0.15}MnO_3$ | $1.4x10^4$ | $1.4x10^4$ | $1.4x10^4$ | $10^{-5}$(900°C) [12] | 11.7 |
| $InO_{1.5}$-30mol%$ZrO_2$ | $1.2x10^4$ | $1.1x10^4$ | $1.0x10^4$ | 1(900°C) [20,21] | 10.1 [17] |
| $InO_{1.5}$-5mol%$SnO_2$ | $5.4x10^4$ | $5.3x10^4$ | $5.4x10^4$ | $5x10^{-1}$(723°C) [18,22] | 9 [23] |
| $La_{0.5}Sr_{0.5}CoO_3$ | $3.4x10^4$ | $3.8x10^4$ | $4.4x10^4$ $4.7x10^4$ [5] | $8x10^1$(900°C) [12] ($La_{0.6}Sr_{0.4}CoO_3$) | 22.0 |
| $La_{0.3}Sr_{0.7}CoO_3$ | - | - | $4x10^4$ [5] | | 15.6 |
| $La_{0.7}Sr_{0.3}CoO_3$ | - | - | $3x10^4$ [5] | | 18.3 |
| $La_{0.8}Sr_{0.2}Co_{0.8}Fe_{0.2}O_{3-\delta}$ | - | $2x10^4$ [24] | $2x10^4$ [24] | $1x10^1$(800°C) [24] | 18.4 |
| $La_{0.2}Sr_{0.8}Co_{0.8}Fe_{0.2}O_{3-\delta}$ | $5.6x10^3$ | $6.3x10^3$ | $8.1x10^3$ $1.5x10^4$ [24] | $1x10^3$(800°C) [16] $1x10^2$(800°C) [24] | 24.0 |
| $ZrO_2$-8mol%$Y_2O_3$ | - | - | - | 11.5 (950°C) 8.57 (900°C) 3.75 (800°C) | 10.5 [17] |

Anodes Ni/YSZ

**Table 2: In-plain resistivity of cathode layers (Ω)@**

| Materials (cathode thickness#) | Co-sintering temperature | | |
|---|---|---|---|
| | 1000°C | 1100°C | 1200°C |
| $La_{0.85}Sr_{0.15}MnO_3$ (50μm) | 5000 | 2000 | 500 |
| 90$InO_{1.5}$-10mol%%$ZrO_2$ (50μm) /70$InO_{1.5}$-30mol%%$ZrO_2$ (15μm) | - | - | 20 (co-sintered at 1375°C) |
| $La_{0.5}Sr_{0.5}CoO_3$ (50μm) | 600 | 60 | 30 |
| $La_{0.5}Sr_{0.5}CoO_3$ (15μm) /$La_{0.5}Sr_{0.5}Mn_{0.5}Co_{0.5}O_3$ (15μm) /$La_{0.85}Sr_{0.15}MnO_3$ (15μm) | - | 10000 | - |
| $La_{0.5}Sr_{0.5}CoO_3$ (50μm) /LSC+8Y-$ZrO_2$ layer (15μm) | 8000 | 60000 | 4000000 |

@2-wire method, point contact with a distance of 2.7 mm
#Cathode thickness before sintering are given.

## IRF SOFC Exploded Schematic with Flows

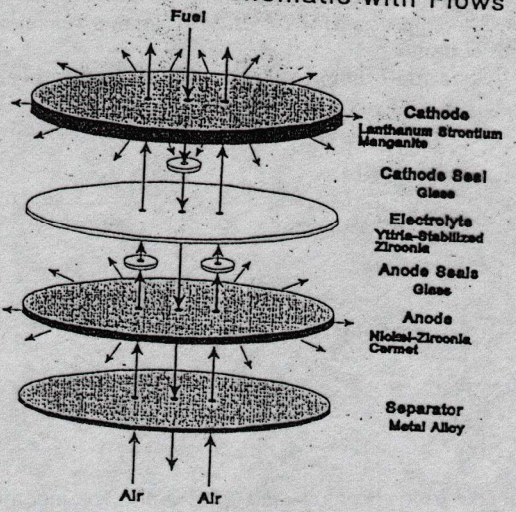


## New Power Generation Options

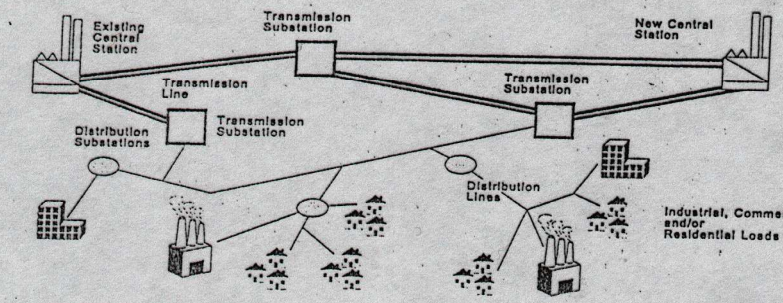


Traditional Expansion

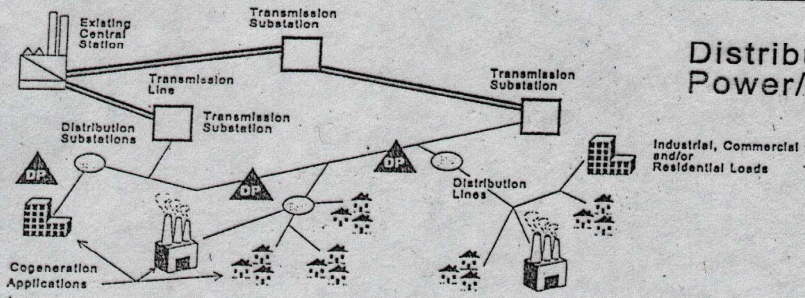


Distributed Power/Cogeneration

M96001064W

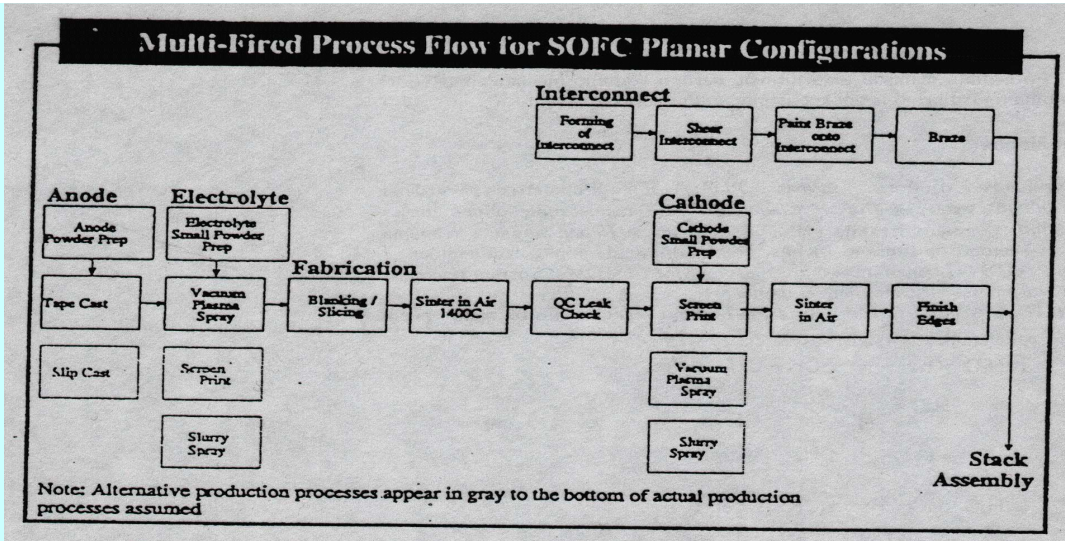


Example of manufacturing process description.

| | Market Segment | Typical Capacity | Allowable Installed Cost[1] ($/kW) Entry[2] | Allowable Installed Cost[1] ($/kW) Sustained[2] |
|---|---|---|---|---|
| On-site | Commercial Cogeneration | 50 kW - 2 MW | $1,500 - 2,000 | $800 - 1,300 |
| On-site | Industrial Cogeneration | 5 - 200 MW | $1,000 - 1,200 | $800 - 1,000 |
| On-site | Residential Power | 0.5 - 10 kW | $1,000 - 2,500 | $800 - 1,000 |
| Utility | Distributed Power | 5 - 20 MW | $1,300 - 1,500 | $800 - 1,300 |
| Utility | Central Station | 100 - 500 MW | $900 - 1,100 | $700 - 900 |

[1] Total installed system costs, including all owners costs. Targets apply widely to industrialized country markets. Costs have been calculated based on a range of electricity and gas rate structures. Allowable costs for hydrogen fueled systems would be considerably lower as merchant hydrogen prices are typically 2-3 times as high as natural gas.
[2] "Entry" costs are based on early high value markets. "Sustained" costs must be realized to achieve significant market penetration.

Summary characterization of potential stationary power markets

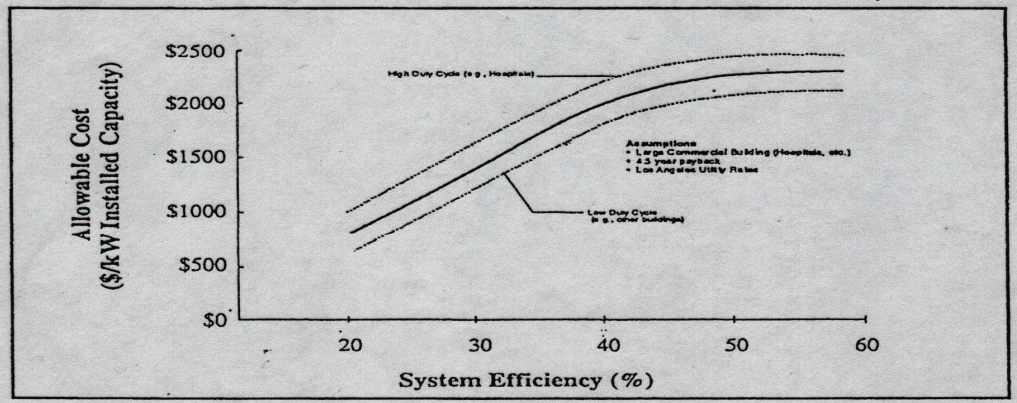


Impact of system efficiency on allowable system cost.

# Chronology of Solid Electrolyte Cells

| Date | Electrolyte | Log (S/cm) | Typical Cell System |
|---|---|---|---|
| 1950-60 | AgI | -5 | Ag/$V_2O_5$ |
| 1960-65 | $Ag_3SI$ | -2 | Ag/$I_2$ |
| 1965-72 | $RbAg_4I_5$ | -0.5 | Ag/$Me_4NI_5$ |
| 1965-75 | Beta-alumina | -1.5 | Na-Hg/$I_2$,PC |
| 1970-75 | LiI($Al_2O_3$) | -5 | Li/$PbI_2$ |
| 1970-80 | LiI | -7 | Li/$I_2$ |
| 1978-85 | LiX-PEO[b] | -7 | Li/$V_2O_5$ |
| 1980-86 | $Li_{0.36}I_{0.14}O_{0.007}P_{0.11}S_{0.38}$ | -3.3 | Li/$TiS_2$ |
| 1983-87 | MEEP[c] | -4 | Li/$TiS_2$ |
| 1985-92 | Plasticized SPE[d] | -3 | Li/$V_6O_{13}$ |
| 1985-92 | $Li_{0.35}I_{0.12}O_{0.31}P_{0.12}S_{0.098}$ | -4.7 | Li/$TiS_2$ |
| 1990-92 | $Li_{0.39}N_{0.020}O_{0.47}P_{0.12}$ | -5.6 | Li/a-$V_2O_5$ |

PEO - Polyetylene oxide

MEEP - Methoxyethyoxyetyoxy polyphosphazene

SPE - Solid polymer electrolyte

# CHEMICAL REACTIONS IN SSB

Anodic reaction:

$Na \leftrightarrow Na^+ + e^-$

$2\,Li \leftrightarrow 2\,Li^+ + 2\,e^-$

or $Li^+ + e^- \leftrightarrow Li$

Cathodic reaction:

$Na^+ + \frac{x}{2} S + e^- \leftrightarrow \frac{1}{2} Na_2S_x$ , kai $x \leq 3$

$2\,Li^+ + 2\,e^- + I_2 \leftrightarrow 2\,LiI$

or $Li\,Co^{3+}O_2 \leftrightarrow Co^{4+}O_2 + Li^+ + e^-$

Total reaction:

$2\,Li + I_2 \leftrightarrow 2\,LiI$

The chemical reactions in the Na/S superionic batteries:

$2Na + 5S \rightarrow Na_2S_5$ - Voltage 2.08 V $\simeq$ 2.1V

$2Na + 4\,Na_2S_5 \rightarrow 5\,Na_2S_4$ - Voltage 1.97 V

$2Na + 3\,Na_2S_4 \rightarrow 4\,Na_2S_3$ - Voltage 1.81 V

The chemical reactions in the Ni-MH cell

$Ni(OH)_2 \leftrightarrow H_x + Ni(OOH)$

$LaNi_5 + H_x \leftrightarrow LaNi_5H_x$

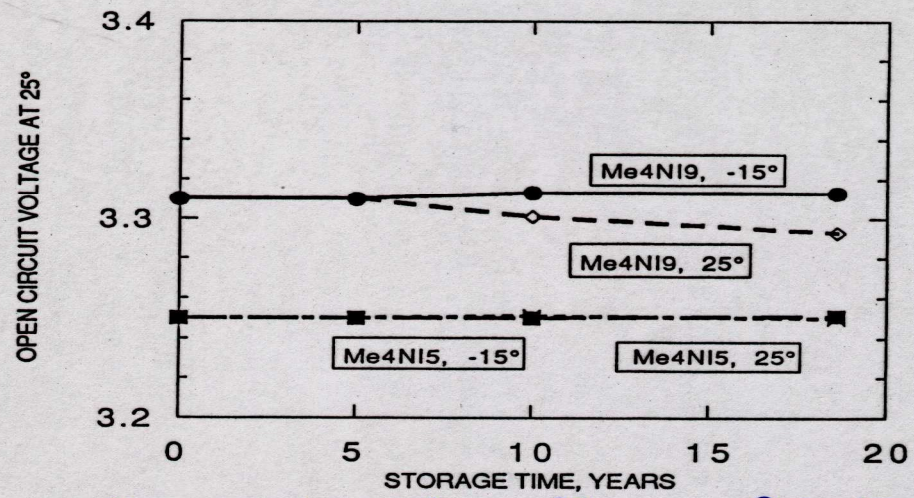


Open circuit voltage of $Ag/I_2$ batteries as function of storage time

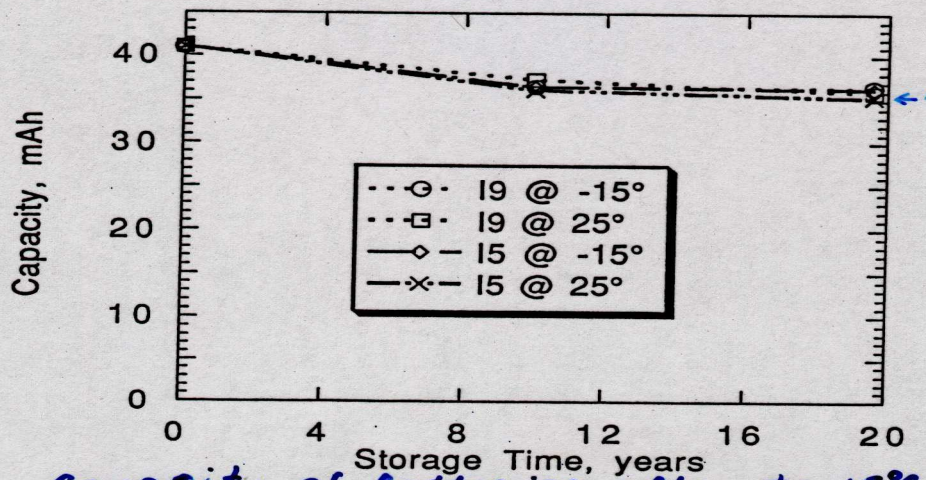


Capacity of batteries after t=-15°C or 25°C storage ($I_9$ - $Ag/Me_4NI_9$, $I_5$ - $Ag/Me_4NI_5$). Batteries were discharged at 25° and 60°C, at a constant load of 64,9 kΩ (30 day rate)

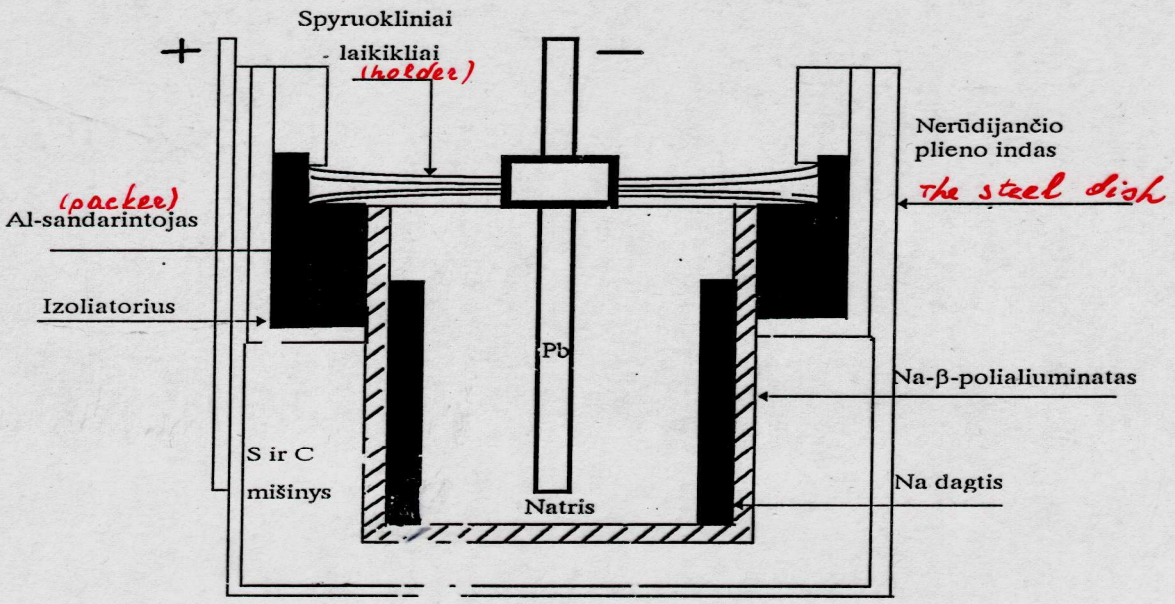
Spyruokliniai
- laikikliai
(holder)
+
−
Nerūdijančio
plieno indas
the steel dish
(packer)
Al-sandarintojas
Izoliatorius
Pb
Na-β-polialiuminatas
S ir C
mišinys
Natris
Na dagtis

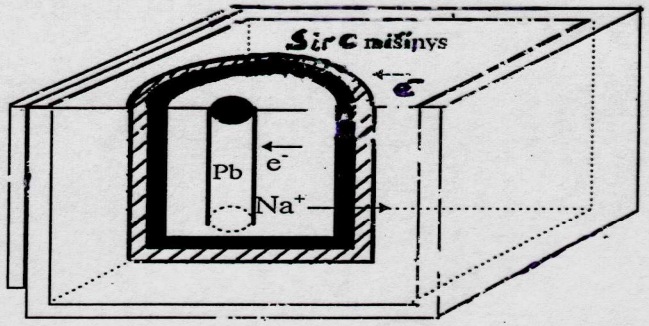
S ir C mišinys
e
Pb
e⁻
Na⁺

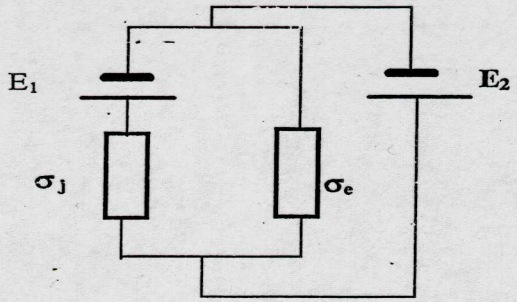
E₁
E₂
σj
σe

Poly-2 vinilpiridinium $I_2$ complex

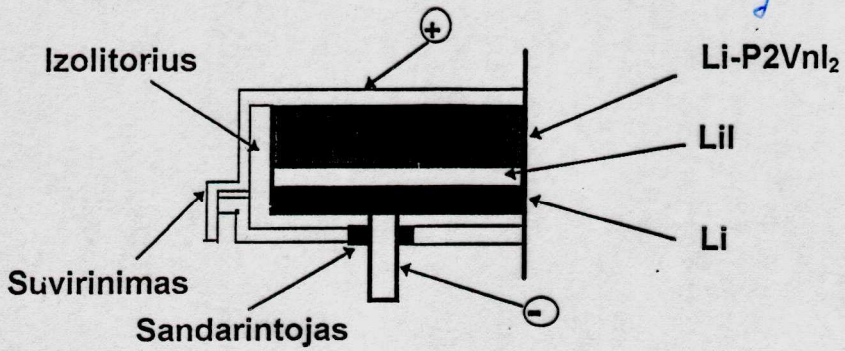


iškrovimas

$x\,Li^+ + Ti\,S_2 \leftrightarrow Li_x\,Ti\,S_2 \quad (0 \leq x \leq 1)$

įkrovimas

storis $d = 40\,\mu m$

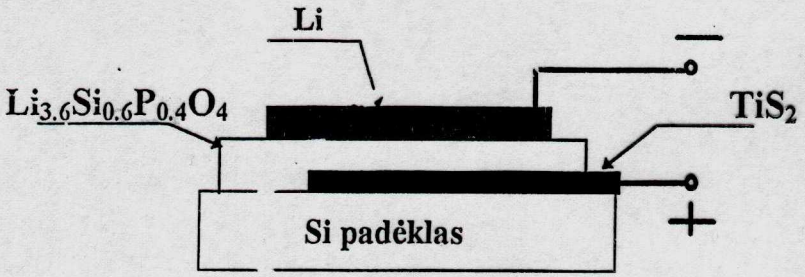

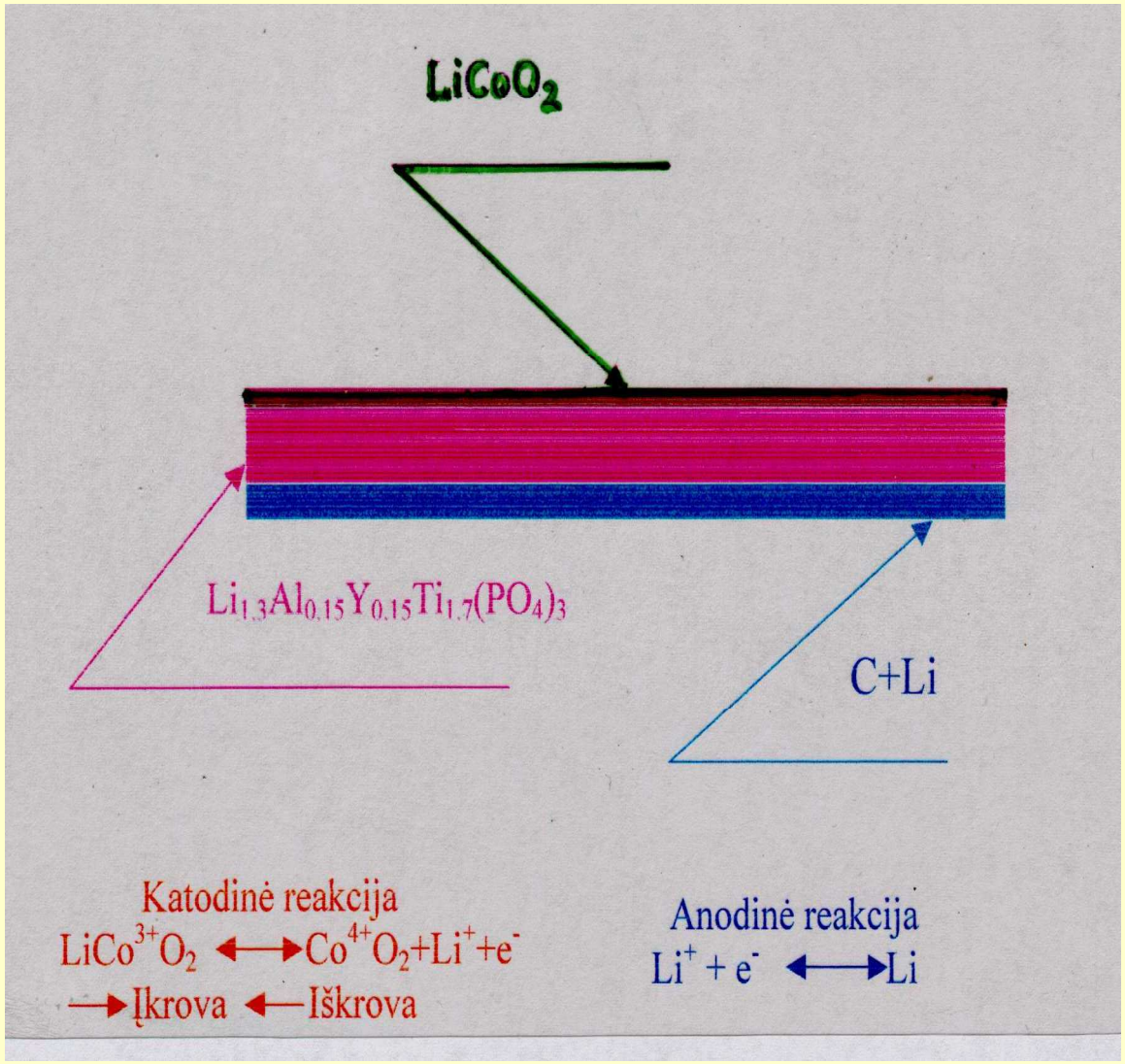
$LiCoO_2$
$Li_{1.3}Al_{0.15}Y_{0.15}Ti_{1.7}(PO_4)_3$
C+Li
Katodinė reakcija
$LiCo^{3+}O_2 \longleftrightarrow Co^{4+}O_2 + Li^+ + e^-$
Įkrova
Iškrova
Anodinė reakcija
$Li^+ + e^- \longleftrightarrow Li$

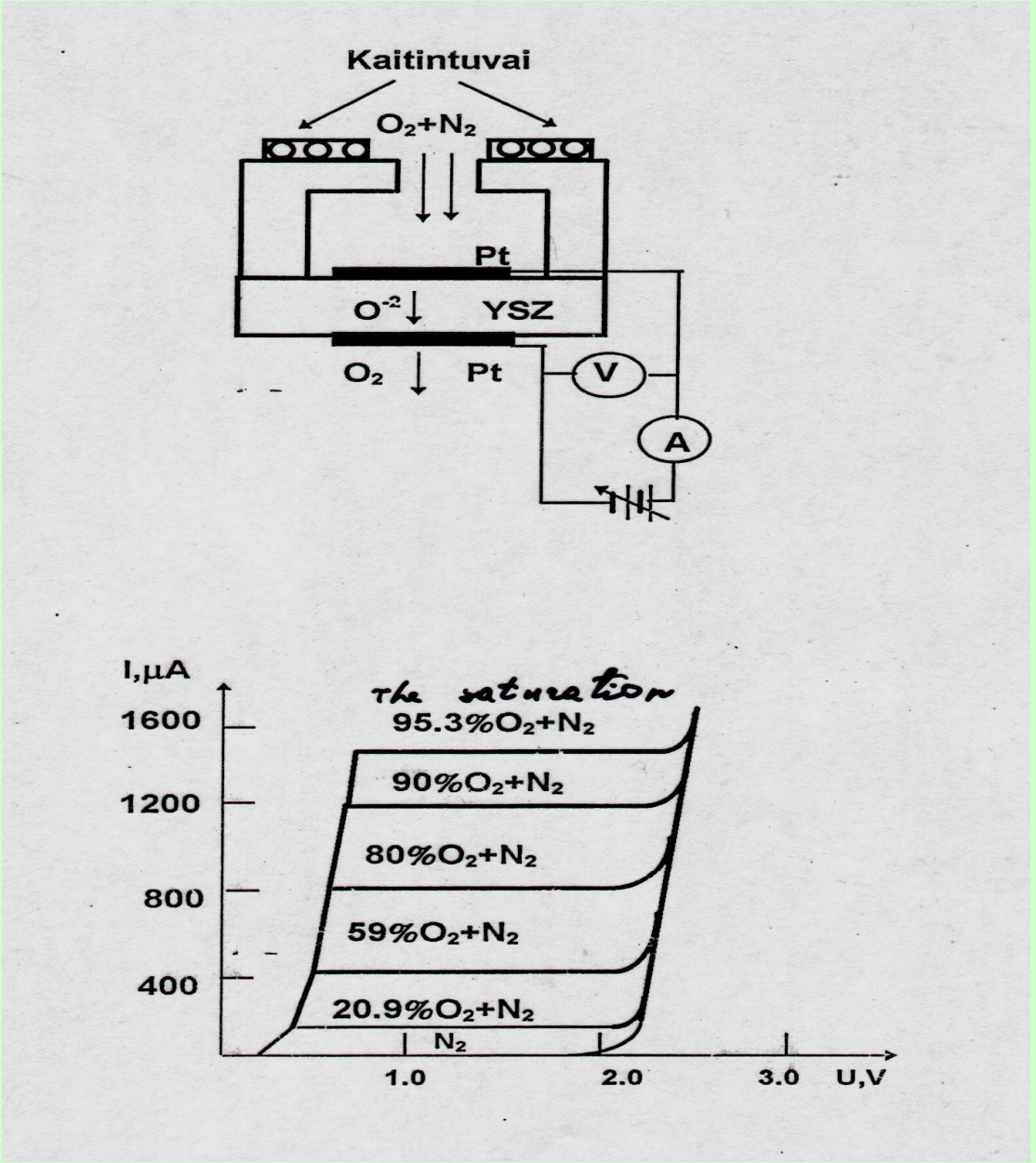
Kaitintuvai
O2+N2
Pt
O-2
YSZ
O2
Pt
V
A
I,μA
1600
1200
800
400
the saturation
95.3%O2+N2
90%O2+N2
80%O2+N2
59%O2+N2
20.9%O2+N2
N2
1.0
2.0
3.0
U,V

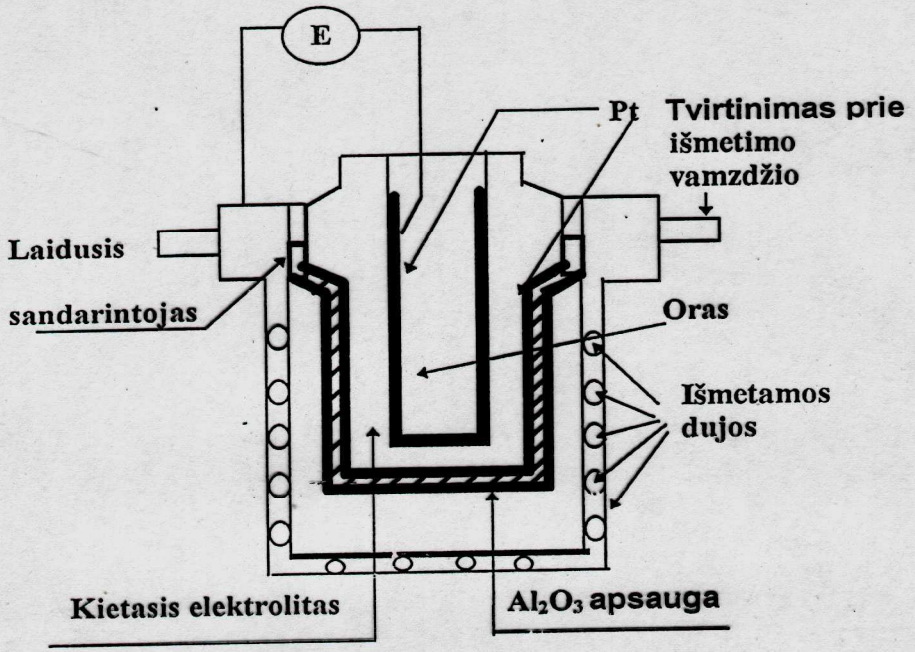


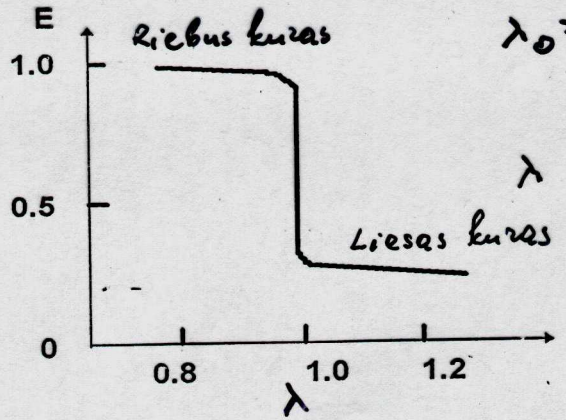


$\lambda_0 = \frac{Air}{Fuel} = 13.7\ g/g$

$\lambda = (A/F)/\lambda_0$

Plokščiojo kondensatoriaus talpa

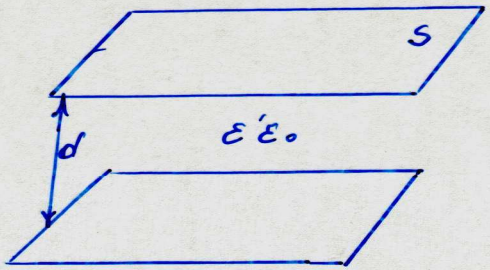


$$C = \frac{\varepsilon' \varepsilon_0 S}{d}$$

Rutulio talpa

$$C = 4\pi \varepsilon' \varepsilon_0 R$$

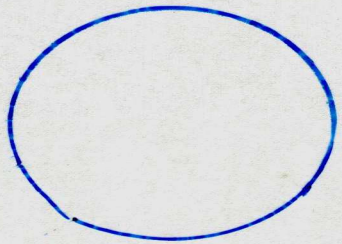

Cilindrinio kondensatoriaus talpa

$$C = \frac{2\pi \varepsilon' \varepsilon_0 l}{\ln\left(\frac{R_2}{R_1}\right)};$$

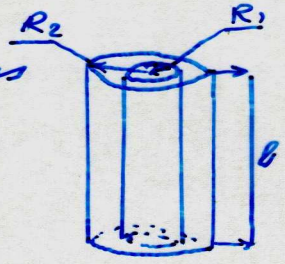


Sferinio kondensatoriaus talpa

$$C = 4\pi \varepsilon \varepsilon_0 \frac{R_1 R_2}{R_2 - R_1}$$

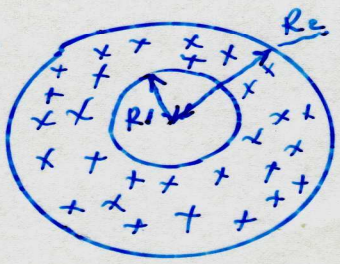

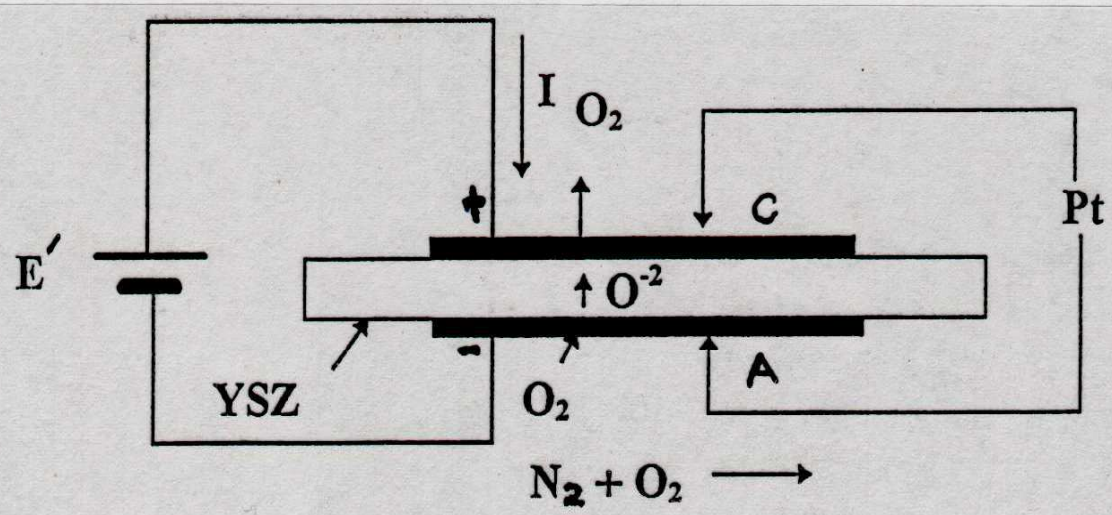


$V \simeq I/4F$ ; $F \simeq 9.65 \cdot 10^7$ C/kg-ekv

$T = 298$ K ; $p = 1$ atm , $I = 1$ A

$v = 3$ ml/min